



Detailed Analysis of the Asteroid Pair (6070) Rheinland and (54827) 2001 NQ8

David Vokrouhlický¹, Petr Pravec², Josef Ďurech¹, Kamil Hornoch², Peter Kušnirák², Adrián Galád², Jan Vraštil², Hana Kučáková², Joseph T. Pollock³, Jose Luis Ortiz⁴, Nicolas Morales⁴, Ninel M. Gaftonyuk⁵, Donald P. Pray⁶, Yuriy N. Krugly⁷, Raguli Ya. Inasaridze⁸, Vova R. Ayvazian⁸, Igor E. Molotov⁹, and Carlos A. Colazo¹⁰

¹Institute of Astronomy, Charles University, V Holešovičkách 2, CZ-180 00 Prague 8, Czech Republic

²Astronomical Institute, Czech Academy of Sciences, Fričova 298, CZ-251 65 Ondřejov, Czech Republic

³Department of Physics and Astronomy, Appalachian State University, 525 Rivers Street, Boone, NC 28608, USA

⁴Instituto de Astrofísica de Andalucía—CSIC, Apt. 3004, E-18008 Granada, Spain

⁵Crimean Astrophysical Observatory, Department of Radioastronomy and Geodynamics, Simeiz, 298680, Crimea[†]

⁶Sugarloaf Mountain Observatory, South Deerfield, MA 01373, USA

⁷Institute of Astronomy of Kharkiv National University, Sumska Str. 35, Kharkiv 61022, Ukraine

⁸Kharadze Abastumani Astrophysical Observatory, Ilia State University, G. Tsereteli str. 3, 0162 Tbilisi, Georgia

⁹Keldysh Institute of Applied Mathematics, RAS, Miusskaya sq. 4, 125047 Moscow, Russia

¹⁰Observatorio Astronómico, Universidad Nacional de Córdoba, Laprida 854, X5000BGR—Córdoba, Argentina

Received 2017 March 31; revised 2017 May 11; accepted 2017 May 11; published 2017 June 1

Abstract

The existence of asteroid pairs, two bodies on similar heliocentric orbits, reveals an ongoing process of rotational fission among asteroids. This newly found class of objects has not been studied in detail yet. Here we choose asteroids (6070) Rheinland and (54827) 2001 NQ8, the most suitable pair for an in-depth analysis. First, we use available optical photometry to determine their rotational state and convex shapes. Rotational pole of Rheinland is very near the south ecliptic pole with a latitude uncertainty of about 10° . There are two equivalent solutions for the pole of 2001 NQ8, either $(72^\circ, -49^\circ)$ or $(242^\circ, -46^\circ)$ (ecliptic longitude and latitude). In both cases, the longitude values have about 10° uncertainty and the latitude values have about 15° uncertainty (both 3σ uncertainties). The sidereal rotation period of 2001 NQ8 is 5.877186 ± 0.000002 hr. Second, we construct a precise numerical integrator to determine the past state vectors of the pair's components, namely their heliocentric positions and velocities, and orientation of their spin vectors. Using this new tool, we investigate the origin of the (6070) Rheinland and (54827) 2001 NQ8 pair. We find a formal age solution of 16.34 ± 0.04 kyr. This includes effects of the most massive objects in the asteroid belt (Ceres, Pallas, and Vesta), but the unaccounted gravitational perturbations from other asteroids may imply that the realistic age uncertainty is slightly larger than its formal value. Analyzing results from our numerical simulation to 250 kya, we argue against a possibility that this pair would allow an older age. Initial spin vectors of the two asteroids, at the moment of their separation, were not collinear, but tilted by $38^\circ \pm 12^\circ$.

Key words: minor planets, asteroids: general

1. Introduction

Families of asteroids, bodies sharing the same zone of orbital proper semimajor axis, eccentricity, and inclination, have long been known in the main belt and interpreted as products of collisional fragmentations of a single parent asteroid. Large and old families were recognized to be less useful to describe details of the initial breakup event. This is because many dynamical and physical processes can modify their orbital architecture, observed spin states or spectral properties of their surfaces. This motivated search for young asteroid families, in which time-dependent processes would have less opportunity to change dynamical and physical parameters of the family members. Discovery of the ≈ 5.75 Myr old Karin family (Nesvorný et al. 2002) represented a breakthrough in this respect. However, even the Karin family shows traces of dynamical evolution (e.g., Nesvorný & Bottke 2004; Carruba et al. 2016). Therefore, a race for still younger families was on. This required a change in strategy of the search: rather than using the proper orbital elements, it became handy to use simpler osculating orbital elements in which very young

families were expected to cluster as well. With this new method, Nesvorný et al. (2006) discovered the Datura family, the first example younger than 1 Myr. However, even the ≈ 0.5 Myr old Datura family was found to be potentially modified by aging processes. For instance, Vernazza et al. (2009) have shown that spectral properties of members in the Datura, and similarly young, families indicate traces of the process generally called space weathering, making them different from meteorite analogs. As a result, the need to discover even younger families was still on.

In response to this evolution, Vokrouhlický & Nesvorný (2008) stumbled over a peculiar class of couples of asteroids residing on extremely similar heliocentric orbits in the main belt and among the Hungaria population. While it was possible that they represent just two of the largest objects in very young asteroid families, thus fulfilling the initial task, Vokrouhlický & Nesvorný (2008) also proposed different explanations. Their favored was the assumption that components in these asteroid pairs were created when a parent body underwent rotational fission (rather than collisional breakup, as in standard families). Thus, while sharing with families the ultimate origin in physical destruction of the parent body, the asteroid pairs likely differ in the primary mechanism driving this catastrophe (see Pravec et al. 2010, for a convincing argument). This way,

[†] While the AAS journals adhere to and respect UN resolutions regarding the designations of territories (available at <http://www.un.org/press/en>), it is our policy to use the affiliations provided by our authors on published articles.

the pairs are genetically related to small asteroid binary or multiple systems rather than to the families (see, e.g., Margot et al. 2015). Obviously, this does not make the asteroid pairs any less interesting objects to be studied, in fact, the opposite is true. Therefore, various aspects of the population of known pairs have recently been studied. Some authors focused on the analysis of spectral similarity of components in the pairs, others studied dynamical aspects of their orbital evolution since their origin. In this paper, we continue the second line of investigation of asteroid pairs, focusing on both orbital and rotational dynamics of their components.

Similar to the asteroids themselves, our knowledge of the population of asteroid pairs is presently incomplete. This is mainly because all of them are small objects, with sizes less than 10 km or so. As a result, today we know only about a hundred or so of these pairs (e.g., Vokrouhlický & Nesvorný 2008; Pravec & Vokrouhlický 2009; Pravec et al. 2010). Unfortunately, in many cases, the smaller component's astrometric data are still poor, and thus its orbit and size estimate are very uncertain. Aside from noting the existence of such pairs, our additional knowledge in these cases (such as determination of its age) is very limited. In this situation, it appears interesting to select some of the most suitable cases and present their analysis as an archetype of a pair.

One such example has already been noted by Vokrouhlický & Nesvorný (2008). It consists of two components, (6070) Rheinland and (54827) 2001 NQ8, moderately large asteroids residing in the inner part of the main asteroid belt. Additionally, the age of this pair has been found to be very young, at only 17 kyr. These facts make this asteroid pair ideal for an in-depth study.

In regards to the past orbital evolution, and consequent reconstruction of the system's initial configuration, and the constraint of its age, we cite the work of Vokrouhlický & Nesvorný (2009), which extended the previous results of Vokrouhlický & Nesvorný (2008). By careful tracking of the multitude of possible realizations of past orbital evolution for both asteroids in this pair, and by taking their mutual gravitational attraction when they come close enough to each other, Vokrouhlický & Nesvorný (2009) were able to find that the 54827 component might have initially rested on the surface of 6070, or resided in a very close satellite orbit. Analyzing the exceptionally well converging cases, these authors noted a preference for retrograde rotation of the larger component 6070. Two years later, Vokrouhlický et al. (2011) assembled enough light-curve observations of 6070 to indeed prove its retrograde sense of rotation. In particular, they showed that the ecliptic latitude of 6070 is smaller than -50° , and quite possibly even -60° , with the ecliptic longitude poorly constrained (because of the obvious geometric degeneracy). Polishook (2014), adding more light-curve observations, confirmed this result. Both references also derived a rough convex approximation of the 6070's shape and noted a possible equatorial asymmetry, which may be a relic of the fission event. Interestingly, Vokrouhlický et al. (2011) further analyzed the past convergence of the two components in the 6070–54827 pair and suggested that also the smaller component, asteroid (54827) 2001 NQ8, should preferentially rotate in a retrograde sense. This is because many more convergent cases were found among realizations when the two asteroids had the same, rather than the opposite, sense of rotation. A confirmation would certainly have interesting implications on the fission mechanics

of the parent body of the pair. We also note that Galád (2012) pointed out that an accurate modeling of the convergence of the 6070 and 54827 orbits in the past requires the inclusion of gravitational perturbations of the most massive asteroids, aside from the obvious effects of planets.

Interesting information about the 6070–54827 pair has also been obtained using spectroscopic observations. The near-infrared data presented by Polishook et al. (2014a) revealed that spectra of both asteroids fall within the S-group. This is consistent with their membership in the large Nysa family (Nesvorný et al. 2015, and the related data files at the PDS website), or the Hertha family (in classification by Milani et al. 2014). Nevertheless, while the spectra of 6070 and 54827 were found to be similar, they are not identical in details. For instance, the spectrum of 6070 was classified as Sq, while that of 54827 is Q. Other spectral features discussed in Polishook et al. (2014a) also indicate that the surface of the secondary component in the pair is less affected by the processes of space weathering. This has been interpreted as a global settling of dust predominantly on the primary component 6070 after the fission event took place. Such a model is also supported by the observation that there is no, or an insignificant, spectral variation of 6070 during its rotation cycle (Polishook et al. 2014b).

The *Wide-field Infrared Survey Explorer* (WISE) spacecraft observations provided additional data, namely the size D and the geometric albedo p_V for (54827) 2001 NQ8 and the neighboring Nysa/Hertha family. However, there are no direct WISE observations of the primary component (6070) Rheinland and those of (54827) 2001 NQ8 are very uncertain. This is because WISE detected this asteroid in a single band only (W3), which provided too limited data set to significantly constrain its D and p_V . Therefore, the formal values $D = 2.08 \pm 0.54$ km and $p_V = 0.21 \pm 0.14$ (Masiero et al. 2011) should be taken with a large grain of caution. We observe that the reported albedo value is consistent with the average value of Hertha members $p_V = 0.28 \pm 0.09$ from Masiero et al. (2013), but we conservatively stick to the lower mean albedo value of 0.20 ± 0.05 found by Pravec et al. (2012) for a generic S- or Q-type asteroids. We believe this is an adequate approximation in our case.

In this paper, we have two principal goals. First, we use light-curve observations of the secondary component (54827) 2001 NQ8 to derive its rotation state and shape (Sections 2 and 3). This is primarily motivated by the aforementioned educated guess in Vokrouhlický et al. (2011) that this asteroid should have a retrograde rotation. Next, having resolved the rotation state for both primary and secondary components in the 6070–54827 pair, we may significantly improve the accuracy of the past orbital evolution of their orbits. New features of our model are described in Section 4, and results are reported in Section 5.

2. Observations

2.1. (6070) Rheinland

Thanks to its larger size, the primary component (6070) Rheinland has been photometrically observed on a number of occasions since Vokrouhlický & Nesvorný (2008) attracted attention to this pair of objects. Early data were summarized in Vokrouhlický et al. (2011), while further observations were published by Polishook (2014). Here we report additional

Table 1
Aspect Data for Observations of (6070) Rheinland

| Date | r (au) | Δ (au) | α (deg) | λ (deg) | β (deg) | Obs. |
|---------------|-------------|------------------|-------------------|--------------------|------------------|------|
| 2012 May 14.3 | 2.673 | 1.683 | 5.4 | 248.1 | 1.8 | P1 |
| 2012 May 19.0 | 2.665 | 1.661 | 3.4 | 247.0 | 1.7 | Aba |
| 2012 May 21.3 | 2.661 | 1.653 | 2.4 | 246.4 | 1.7 | P1 |
| 2012 Jun 17.8 | 2.611 | 1.664 | 10.1 | 239.9 | 1.2 | Aba |
| 2012 Jun 22.8 | 2.601 | 1.687 | 12.2 | 239.0 | 1.1 | Aba |
| 2012 Jun 24.8 | 2.597 | 1.697 | 12.9 | 238.7 | 1.0 | Aba |
| 2013 Oct 27.9 | 1.972 | 1.135 | 20.6 | 78.8 | -2.4 | Aba |
| 2013 Oct 31.1 | 1.977 | 1.117 | 19.3 | 78.6 | -2.3 | LH |
| 2013 Nov 03.3 | 1.982 | 1.101 | 17.8 | 78.3 | -2.2 | P1 |
| 2013 Nov 13.1 | 1.999 | 1.063 | 12.7 | 76.9 | -2.0 | LH |
| 2013 Nov 23.1 | 2.017 | 1.045 | 6.9 | 74.8 | -1.7 | LH |
| 2013 Nov 24.0 | 2.019 | 1.044 | 6.3 | 74.5 | -1.6 | Sim |
| 2013 Nov 26.1 | 2.022 | 1.044 | 5.0 | 74.0 | -1.6 | LH |
| 2013 Dec 04.0 | 2.038 | 1.052 | 0.6 | 72.0 | -1.3 | Ond |
| 2013 Dec 06.0 | 2.042 | 1.057 | 1.3 | 71.5 | -1.2 | LH |
| 2013 Dec 12.8 | 2.055 | 1.080 | 5.2 | 69.8 | -0.9 | Sim |
| 2013 Dec 20.9 | 2.072 | 1.123 | 9.7 | 68.1 | -0.6 | Ond |
| 2013 Dec 21.8 | 2.074 | 1.129 | 10.2 | 68.0 | -0.6 | Ond |
| 2013 Dec 21.9 | 2.074 | 1.129 | 10.3 | 68.0 | -0.6 | Aba |
| 2014 Jan 30.1 | 2.161 | 1.521 | 23.9 | 67.4 | 0.6 | SM |

Note. We report here our new observations only; the complete data set also includes additional observations reported in Vokrouhlický et al. (2011) and Polishook (2014). The table gives the asteroid's UTC epoch of the mid-time of the observational run, distance from the Sun r and from the Earth Δ , the solar phase angle α , the geocentric ecliptic coordinates of the asteroid (λ , β), and the observatory (P1—PROMPT 1, 41 cm; Aba—Abastumani, 70 cm; LH—La Hita, 77 cm; Sim—Simeiz, 1 m; Ond—Ondřejov observatory, 65 cm; SM—Sugarloaf Mountain, 50 cm).

observations performed during the 2012 and 2013–2014 oppositions (Table 1). In total, we have 4021 data points (individual photometric observations) of this asteroid.

Several light curves were obtained at PROMPT using a 0.41 m Ritchey–Chrétien telescope equipped with Apogee Alta U47+ camera located at Cerro Tololo Inter-American Observatory in Chile. Images were dark and bias subtracted and flat fielded using the photometric reduction program MIRA. MIRA was then used as well to conduct aperture photometry on the object and several comparison stars in the field.

The observations at the Abastumani Astrophysical Observatory were carried out with the 0.7 m meniscus Maksutov telescope with FLI IMG6303E CCD camera in the primary focus ($f/3$). Observational method and reduction procedures at Abastumani were the same as those we used at Simeiz observatory (see below). The observations were made without a filter.

The observations at the Simeiz observatory were carried out with a 1-m Ritchey–Chrétien telescope at Simeiz Department of the Crimean Astrophysical Observatory using camera FLI PL09000. The observations were made in the Johnson–Cousins photometric system. The standard procedure of image reduction included dark removal and flat-field correction. The aperture photometry was done with the AstPhot package described in Mottola et al. (1995). The differential light curves were calculated with respect to an ensemble of comparison stars by the method described in Erikson et al. (2000) and Krugly (2004).

The observations at the La Hita observatory (Toledo, Spain) were carried out using a 0.77 m $f/3.3$ telescope equipped with a

peltier-cooled $4K \times 4K$ SBIG STX16803 CCD camera. This camera has a corrected field of $48'1 \times 48'1$ and a plate scale of 0.705 arcsec/pixel. The image sequences were acquired with no filter in order to maximize the signal-to-noise. Calibration images such as dark frames, bias frames, and sky flat fields were obtained each night. The science images were dark-subtracted and flat fielded using the calibration frames and standard procedures. The synthetic aperture photometry was obtained with the same methods and techniques as for the Ondřejov observations.

Observational system, data analysis, and reduction process at the Ondřejov observatory were identical to those described in Pravec et al. (2006).

Observations at Sugarloaf Mountain Observatory were made using a 0.5 m, $f/4.0$ reflector on a Paramount ME mount. The imaging CCD was an SBIG ST-10XME cooled to -15°C , where images were taken through a clear filter. The image scale was 1.38 arcsec/pixel, and the fov was 25.0×16.8 arcmin. Derived magnitudes were estimated using a method inherent in the analysis software, MPO Canopus. The method is based on referencing a hybrid star catalog consisting mostly of 2MASS stars in the V band. Images were calibrated using master bias, dark, and flat-field images.

The Ondřejov observations, and those reported in Vokrouhlický et al. (2011), were absolutely calibrated in the Cousins R photometric system. Using the HG system parametrization of the phase function allowed us to determine absolute magnitude $H_{1,R} = 13.67 \pm 0.02$ and the slope parameter $G = 0.27 \pm 0.03$ (see also Vokrouhlický et al. 2011). Using the color index $(V - R) = 0.49 \pm 0.05$, appropriate for S- and Q-type asteroids (see, e.g., Pravec et al. 2012), and the abovementioned assumption about the geometric albedo value, we obtain an estimated $D_1 = 4.4 \pm 0.6$ km for the size of the primary component in our pair.

2.2. (54827) 2001 NQ8

Previous photometry of (54827) 2001 NQ8, from its favorable opposition in 2009, has been described in the supplementary materials of Pravec et al. (2010). In this paper, we report additional observations from the four oppositions in 2012, 2013–2014, 2015, and 2016. Altogether we thus dispose of 14 new light curves whose observation details, such as the aspect data, heliocentric and observer distances, and observing stations are given in Table 2. The total number of data points (individual photometric observations) is 948 for this asteroid. The observations in the 2013–2014 and 2016 oppositions each extend over three lunations, which allows us to uniquely link the rotation phase angle. This is important to unambiguously determine the sidereal rotation period of the asteroid rotation, a starting point for further analysis of the rotation pole orientation and shape modeling.

For observations with the Danish 1.54 m telescope, we used the same or analogous procedures as those we used for observations from Ondřejov (see above) and for observations of Apophis (Pravec et al. 2014).

The observations taken in 2013–2014, which were obtained at near-equator on aspects, were absolutely calibrated in the Johnson–Cousins VR photometric system and we derived the mean absolute magnitude $H = 15.69 \pm 0.04$ and the slope parameter $G = 0.29 \pm 0.03$. We also measured the color index $(V - R) = 0.424 \pm 0.020$, which is consistent with the Q classification by Polishook et al. (2014a). Together with our

Table 2
Aspect Data for Observations of (54827) 2001 NQ8

| Date | r (au) | Δ (au) | α (deg) | λ (deg) | β (deg) | Obs. |
|---------------|-------------|------------------|-------------------|--------------------|------------------|------|
| 2012 Jul 13.3 | 2.257 | 1.241 | 1.6 | 288.6 | -2.5 | EABA |
| 2013 Dec 09.3 | 2.354 | 1.687 | 21.0 | 135.9 | 2.2 | DK |
| 2014 Jan 24.2 | 2.460 | 1.479 | 2.3 | 128.6 | 3.5 | DK |
| 2014 Jan 31.2 | 2.476 | 1.493 | 2.2 | 126.8 | 3.6 | DK |
| 2014 Feb 24.1 | 2.528 | 1.645 | 12.6 | 121.6 | 3.7 | DK |
| 2015 Mar 20.3 | 2.873 | 2.072 | 13.9 | 223.0 | 3.6 | DK |
| 2015 Mar 27.3 | 2.869 | 2.004 | 11.9 | 222.2 | 3.6 | DK |
| 2015 Mar 30.2 | 2.868 | 1.978 | 10.9 | 221.8 | 3.6 | DK |
| 2016 Aug 23.0 | 1.940 | 0.982 | 13.5 | 356.0 | -6.1 | Ond |
| 2016 Aug 27.0 | 1.935 | 0.962 | 11.4 | 355.4 | -6.2 | Ond |
| 2016 Sep 22.0 | 1.906 | 0.912 | 5.8 | 350.2 | -6.6 | Ond |
| 2016 Sep 22.9 | 1.906 | 0.913 | 6.3 | 350.0 | -6.5 | Ond |
| 2016 Oct 23.1 | 1.887 | 1.037 | 21.3 | 346.6 | -5.5 | DK |
| 2016 Nov 28.1 | 1.885 | 1.347 | 30.1 | 352.8 | -3.8 | DK |

Note. We report here our new observations only; the complete data set also includes additional observations from 2009 November reported in the supplementary section of Pravec et al. (2010). The table gives asteroid’s UTC epoch of the mid-time of the observational run, distance from the Sun r and from the Earth Δ , the solar phase angle α , the geocentric ecliptic coordinates of the asteroid (λ , β), and the observatory (EABA—Estacion Astrofisica de Bosque Alegre, Argentina, 1.54 m; DK—Danish telescope, La Silla, Chile, 1.54 m; Ond—Ondřejov observatory, 65 cm).

assumption about the geometric albedo mentioned in Section 1, we thus obtain a size estimate $D_2 = 2.2 \pm 0.3$ km. Consequently, the size ratio q of the two components in this pair is $q = D_2/D_1 = 0.494 \pm 0.014$.

Combining the size estimate of the two asteroids, and assuming that there are no other components that were produced during the fission of the parent body (see also the discussion in Section 6), we obtain an estimate of the parent body size $D_{\text{par}} = 4.6 \pm 0.6$ km. Observing that neither (6070) Rheinland nor (54827) 2001 NQ8 are strongly elongated bodies, we used simple spherical models to obtain the result. Assuming next the bulk density of 2.3 ± 0.3 g cm $^{-3}$ (e.g., Carry 2012), we obtain the following estimate of the escape velocity from the parent body $V_{\text{esc}} = 2.6 \pm 0.4$ m s $^{-1}$ and the radius of its Hill sphere $R_{\text{Hill}} = 940 \pm 140$ km.

3. Pole and Shape Modeling

We used the light-curve inversion method of Kaasalainen & Torppa (2001) and Kaasalainen et al. (2001) to derive shape, sidereal rotation period, and spin axis direction for both components in the 6070–54827 pair from the available¹¹ data described in Section 2. We assume the body rotates about the shortest axis of the inertia tensor, which is fixed in the inertial space. We keep the discussion of the (6070) Rheinland to minimum level, because the spin state and shape models have already been published in the literature. Our analysis of (54827) 2001 NQ8 is new.

3.1. (6070) Rheinland

Numerous photometric observations of (6070) Rheinland allowed Vokrouhlický et al. (2011) and Polishook (2014) to

¹¹ The whole data set of observations, parameters of the shape model and further information is available from the DAMIT database at <http://astro.troja.mff.cuni.cz/projects/asteroids3D/web.php> (see also Durech et al. 2010).

derive the rotation state of this asteroid. Both references showed that its spin is oriented very near the southern ecliptic pole. In this paper, we used all previous data plus our own additional observations described in Section 2.1 to determine the rotation state and shape of (6070) Rheinland anew.

Not surprisingly, our results confirm the previous analyses. Our formally best-fit solution has a sidereal rotation period of $P = (4.2737137 \pm 0.0000005)$ hr and pole orientation $(\lambda, \beta) = (124^\circ, -87^\circ)$ (ecliptic longitude and latitude). Because the formal rotational pole of Rheinland is so close to the southern ecliptic pole, the latitude and longitude values are not suitable parameters to express its uncertainty. Rather, in Figure 1, we show a map of a statistical quality of the light-curve fit for any convex shape with the rotational pole oriented to a given direction on the sky. The color coding indicates the best achievable normalized χ^2 value: the dark blue regions provide acceptable solutions, and the green and red regions are incompatible with the observations. To estimate the confidence interval from the χ^2 map, we used the same approach as in Vokrouhlický et al. (2011). In particular, we estimated the formal 3σ interval of solutions such that the χ^2 was lower than the value $\chi_{\text{min}}^2 \times (1 + 3\sqrt{2\nu})$, where χ_{min}^2 was the minimum χ^2 for the best-fitting model and ν was the number of degrees of freedom (i.e., 3934 for Rheinland and 861 for 2001 NQ8). The region near the southern ecliptic pole bounded by the white line indicates the estimated 3σ confidence zone for the pole orientation. Basically, all ecliptic longitudes are possible and the latitude is confined to values approximately $\leq -60^\circ$. Consequently, the obliquity of Rheinland’s pole is $\simeq 178^\circ$ with about 10° uncertainty.

We used our nominal shape model of (6070) Rheinland to determine its dynamical ellipticity $\Delta = \left[C - \frac{1}{2}(A + B) \right] / C$, with (A, B, C) principal moments of the inertia tensor. Using the formulation in Dobrovolskis (1996), we obtained $\Delta \simeq 0.26$. Previous experience, however, shows that this value has only $\simeq 20\%$ accuracy (e.g., Vraštil 2015; Vraštil & Vokrouhlický 2015). This is a consequence of at least several factors: (1) the uncertainty of the photometric data, and possibly the correlated fit of the spin state mapped onto the uncertainty of the shape solution, (2) the convex approximation of the asteroid’s real shape, and (3) the assumption of uniform density in the body.

3.2. (54827) 2001 NQ8

There are two possible solutions for the pole of this asteroid. Our best-fit solution P1 has a sidereal rotation period $P = (5.877186 \pm 0.000002)$ hr and rotation pole at $(\lambda, \beta) = (72^\circ, -49^\circ)$, where λ and β are ecliptic longitude and latitude. A similarly good fit is provided by the solution P2 with the same rotation period and rotation pole at $(\lambda, \beta) = (242^\circ, -46^\circ)$. Both solutions have $\simeq 10^\circ$ uncertainty in the ecliptic longitude and $\simeq 15^\circ$ in the ecliptic latitude (both formal 3σ values). Figure 2 shows the statistical quality of the pole solution for (54827) 2001 NQ8 projected onto the whole sky. Given the very small inclination of the asteroids’ orbit (see Table 3), we note that the obliquity of (54827) 2001 NQ8 is $138^\circ \pm 10^\circ$, significantly different from that of (6070) Rheinland.

Figure 3 shows a sample of light-curve data compared to the model. The variable amplitude of the light curves at different oppositions is due to the changing mutual geometry of the Sun,

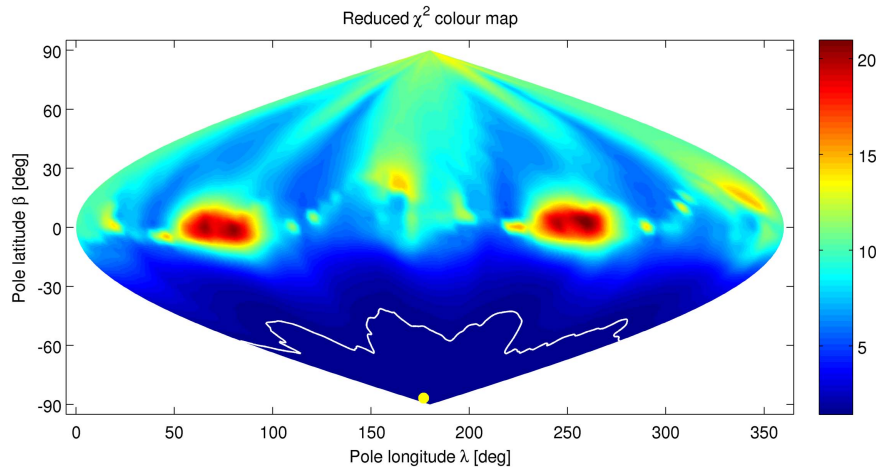


Figure 1. Statistical quality of Rheinland’s pole solutions shown in a sinusoidal projection of the sky in ecliptic coordinates. The color coding, and the scale bar on the right, indicates the value of χ^2 value normalized by the number of observations. The globally best-fit solution at $(\lambda, \beta) = (124^\circ, -87^\circ)$ (full circle) has $\chi^2 = 1.4$ (normalized by the 4021 data points). The solid line delimits solutions within the formal 3σ confidence zone and represents our region of admissible solutions (see the main text for details).

observer, and pole orientation of the asteroid and helps to confine the pole solutions. The uncertainty of the pole direction of (54827) 2001 NQ8 is smaller than for Rheinland because the geometry was not limited to the equatorial plane. For instance, the small amplitude of the 2009 light curve (Figure 3 top and left panel) has to do with only $\simeq 35^\circ$ difference between the line of sight to the asteroid and the pole. Conversely, the much larger amplitude of the 2016 light curve (Figure 3 bottom and right panel) occurs when the difference between the line of sight to the asteroid and the pole is $\simeq 100^\circ$. Figure 4 shows three perpendicular views on the convex shape model of (54827) 2001 NQ8 corresponding to the best-fit solution of the P2 pole. The asteroid’s slight elongations result in a formal value of the dynamical ellipticity $\Delta \simeq 0.24$. The shape solution for the P1 pole provides very similar results.

The photometric data of (54827) 2001 NQ8 could be fit with a model rotating about the shortest axis of the inertia tensor. This implies that its rotation axis is not wobbling in the body frame, or the degree of wobbling is very small (and thus is not detectable with our data). We find this interesting because the canonical estimate of a large-scale tumbling dissipation for a body of this size and rotation period would give a timescale of $\simeq 1.3$ Myr (e.g., Pravec et al. 2014). This is nearly two orders of magnitude larger than the nominal age of the pair (Section 5). The most plausible explanation consists of a very gentle separation of the two components in this pair that did not result in excitation of tumbling for either of them. While this result has been noticed for the primary (larger) components in the pairs, the case of the secondary (smaller) components has not been available so far (see Polishook 2014, for a few exceptions).

4. Age Determination

The above obtained constraint of the pole orientation for both components, (6070) Rheinland and (54827) 2001 NQ8, may help us to refine the determination of their age using the backward integration of orbits in this pair. This is because their known obliquity importantly constrains the value of the Yarkovsky effect, one of the two factors that limit our ability to accurately reconstruct their past orbital configuration. This motivates us to formulate and apply a more advanced dynamical model than was used so far. Some other aspects of the general approach for the

age determination of a given pair of asteroids remain unchanged and could be found, for instance, in Vokrouhlický & Nesvorný (2008, 2009) and Vokrouhlický et al. (2011). Here we primarily focus on novel features or aspects directly relevant for their understanding.

The holy grail of the pair analysis is to reconstruct the configuration of the two bodies right after their separation in the past. If this was achieved, we would also know the moment in history when it happened, and, thus the age of the pair. In an ideal world, this information would be achieved by (1) considering the precise orbit configuration of the two asteroids at present, and (2) by precise orbit propagation of the two orbits into the past. Neither (1) nor (2) are available, and our work needs to account for these intrinsic inaccuracies.

Finite accuracy of astronomical observations, optical astrometry in our case, is the source of problems with (1). As a result, a dynamical state, such as the heliocentric orbital elements at any epoch, determined from the observations, are never known to an infinite accuracy. Rather, the observation uncertainty maps in a certain way onto the determination of the orbital elements (see, e.g., Milani & Gronchi 2010). The best-fit orbital solution has the largest statistical weight, but many orbits in its vicinity in the orbit-element space are still possible solutions, compatible with the statistical uncertainties of the observations. Therefore, we cannot reject them as possible starting conditions of our numerical integrations. In accordance with tradition, these statistically equivalent realizations of orbital initial conditions are called clones.

The currently best-fit osculating orbits of both (6070) Rheinland (primary) and (54827) 2001 NQ8 (secondary), derived from the available astrometric observations, are given in Table 3. These data were taken from AstDyS database provided by the University of Pisa (see <http://hamilton.dm.unipi.it/astdys/>). Both orbits are fairly well constrained at a comparable level, reflecting that both asteroids have been observed over many oppositions and hundreds of astrometric measurements are available for each of them. Table 3 gives information about the formal uncertainty of the six orbital osculating elements $\mathbf{E} = (a, h, k, p, q, \lambda)$, but the complete solution obviously provides also the full normal matrix Σ of the orbital fit, from which mutual correlations of orbital

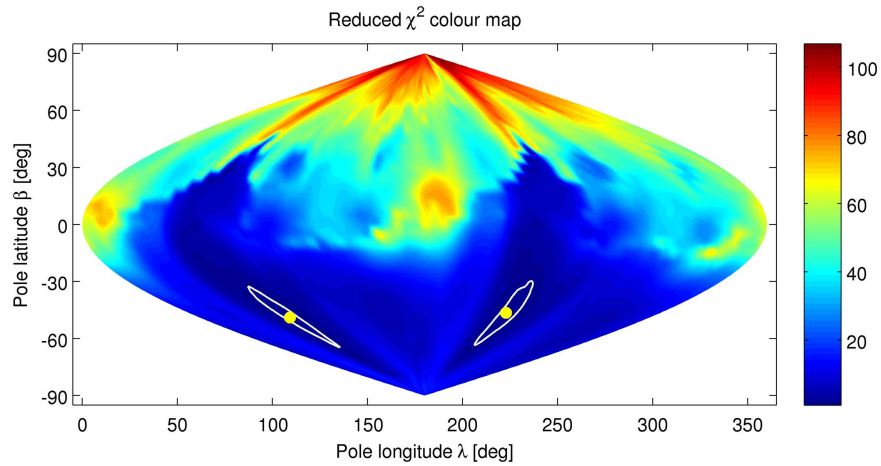


Figure 2. Statistical quality of 2001 NQ8’s pole solutions shown in a sinusoidal projection of the sky in ecliptic coordinates. The color coding and the scale bar on the right indicate the value of the χ^2 value normalized by the number of observations. The globally best-fit solutions at $(\lambda, \beta) = (72^\circ, -49^\circ)$ and $(\lambda, \beta) = (242^\circ, -46^\circ)$ (full circles) have $\chi^2 = 1.7$ (normalized by the 948 data points). The solid line delimits solutions within the formal 3σ region of admissible solutions. These imply conservative estimates of about 10° uncertainty in ecliptic longitude and 15° uncertainty in ecliptic latitude.

parameters can be derived. Only the knowledge of a complete form of Σ eventually provides a key to construct admissible clones for each of the two components in our asteroid pair. In particular, the initial orbital elements of the clones \mathbf{E} are determined using

$$\mathbf{E} = \mathbf{T}^T \mathbf{z} + \mathbf{E}_*, \quad (1)$$

where \mathbf{z} is a six-dimensional vector whose components are random deviates of normal distribution (with variance equal to unity) and \mathbf{E}_* are the best-fit solution from Table 3. The matrix \mathbf{T} satisfies $\mathbf{T}^T \mathbf{T} = \Sigma$ and is obtained using the Cholesky decomposition method. In our production runs, reported in Section 5, we typically used a couple thousand clones of the initial orbital conditions for each of the components in the 6070–54827 asteroid pair. For sake of reference, we note that the initial Cartesian location regions of clones for both primary and secondary components in our pair are similar in size. In particular, they occupy a triaxial-ellipsoid zone with a long axis of about 450 km, and the two short axes of about 100 km. Note that the long axis is comparable to the Hill radius of the parent body of the 6070–54827 asteroid pair already at the current epoch. Obviously, orbit propagation into the past makes it quickly stretch to much larger values (Section 5).

Having the initial data, we can now turn our attention to the orbital propagation of each of the clones into the past. This is the issue (2) mentioned above. The software package `swift` includes gravitational effects of major bodies in the solar system: the Sun and the planets. Given the results in Galád (2012), we also include gravitational perturbations from the dwarf planet Ceres, and the largest asteroids Vesta and Pallas. Their nominal orbital states were taken from `AstDyS` site and their masses were set to 9.384×10^{20} kg (Ceres; Russell et al. 2016), 2.59076×10^{20} kg (Vesta; Russell et al. 2012), and 2.06×10^{20} kg (Pallas; Konopliv et al. 2011). All bodies are considered point masses and Newtonian limit of gravitational interactions are used. The leading, secular post-Newtonian effect is the famous pericenter precession (e.g., Will 1993) that in time T results in a transverse displacement $\tau \simeq 3R_{\text{Sch}} nT$. Here, $R_{\text{Sch}} \simeq 3$ km is the solar Schwarzschild radius and n is the asteroid mean motion. This effect is quite large in

$T \simeq 17$ kyr. However, what matters in our integrations is not τ itself, but the relative displacement of the two components in the pair. Let δa be the mean difference in the semimajor axis values of the two asteroids over the relevant time period T , we have $\delta\tau \simeq \frac{3}{2}\tau(\delta a/a)$. With $\delta a \simeq 3 \times 10^{-5}$ au, appropriate for our studied pair 6070–54827, we obtain $\delta\tau \simeq 5$ km. This is the order of magnitude of the leading post-Newtonian effect in the convergence simulations of 6070 and 54827. Since the periodic effects are about the same order of magnitude as $\delta\tau$, or smaller, we can presently neglect relativistic effects in our analysis.

However, significant orbital perturbations are also produced by effects of a non-gravitational origin. The thermal (self-) acceleration, known as the Yarkovsky effect (e.g., Bottke et al. 2006; Vokrouhlický et al. 2015), is the most important in this class and needs to be included in our simulations. The Yarkovsky effect is caused by recoil of thermally radiated sunlight, that was previously absorbed by the asteroid surface. As a result, the exact value of the thermal acceleration depends on a number of geometrical and physical parameters, such as the asteroid size, rotation state, surface thermal inertial, bulk density etc. Numerous models of various accuracy have been developed to determine the Yarkovsky effect in the past decade or so; however, only the crudest of them were used in modeling past orbital evolution of asteroids in pairs. In what follows, we introduce a model that significantly improves previous approaches.

4.1. New Features of the Model: Thermal Accelerations

All previous efforts to reconstruct the initial configuration of asteroid pairs, and therefore to determine their age, used a simplified model of the thermal accelerations. This is because the virtually zero knowledge of the physical parameters of the two asteroids in the pair, usually small bodies, did not motivate or justify any complex model. Instead, one typically estimated maximum range of secular drift in heliocentric semimajor axis due to the Yarkovsky effect and replaced full representation of the thermal accelerations with only a faked transverse acceleration that produced the same secular effect (see, e.g., Farnocchia et al. 2013). By using this method, short-term orbital perturbations are not properly modeled, and this approximation may produce position errors of several hundreds

Table 3
Osculating Orbital Elements, Their Uncertainties, and Other Parameters of the Asteroid Pair (6070) Rheinland and (54827) 2001 NQ8

| Asteroid | | a (au) | h | k | p | q | λ (deg) | H (mag) |
|---|-----------|-------------|------------|------------|------------|------------|--------------------|--------------|
| 6070 | Rheinland | 2.387462342 | 0.06067382 | 0.20256341 | 0.02716549 | 0.00287963 | 6.4153051 | 14.16 |
| 54827 | 2001 NQ8 | 2.387491801 | 0.06001777 | 0.20262110 | 0.02716017 | 0.00286562 | 41.9179598 | 15.69 |
| <i>Uncertainty</i> ($\delta a, \delta h, \delta k, \delta p, \delta q, \delta \lambda, \delta H$) | | | | | | | | |
| 6070 | Rheinland | 1.0e-8 | 4.8e-8 | 5.5e-8 | 4.2e-8 | 4.5e-8 | 7.2e-6 | 0.05 |
| 54827 | 2001 NQ8 | 8.9e-9 | 4.1e-8 | 6.0e-8 | 3.4e-8 | 5.3e-8 | 5.1e-6 | 0.04 |

Note. Osculating orbital elements and their uncertainty from the `ASTDYS` site and for epoch MJD 57800 (using all astrometric data as of 2016 November). We use a heliocentric equinoctial system of non-singular elements: a is the semimajor axis, $(h, k) = e(\sin \varpi, \cos \varpi)$ where e is the eccentricity and ϖ is the longitude of perihelion, $(p, q) = \tan(i/2)(\sin \Omega, \cos \Omega)$ where i is the inclination and Ω is the longitude of node, and $\lambda = \varpi + M$ is the mean longitude in orbit (M is the mean anomaly). The default reference system is that of the mean ecliptic of J2000. The absolute magnitude, and its uncertainty, in the last column are from our photometric observations.

of kilometers (see a rough estimation by Vokrouhlický & Nesvorný 2008). While small, this is actually of the same order as the typical Hill radius of the parent objects in the pairs. Thus the mismodeling is actually significant and it motivates efforts to improve the propagation model.

Given our knowledge of the spin vectors for both asteroids in the 6070–54827 pair, and our fair constraint of their size, we may now move forward in modeling the thermal accelerations using a more realistic and accurate model. This is presented for the first time in the literature, but we expect that the future astronomical observations will provide necessary information for many other asteroid pairs and our model should become a standard tool.

The model is based on Vokrouhlický et al. (2000), which itself uses the linear solution of the heat conduction in a spherical body from Vokrouhlický (1998, 1999) and Vokrouhlický & Farinella (1999). Even more sophisticated models, taking into account the nonlinear boundary condition when solving heat conduction and irregular shape, were developed for the interpretation of accurate Yarkovsky detections (e.g., Chesley et al. 2003, 2014), but these are not needed here for this calculation. Because the thermal inertia of small asteroids is typically few hundreds in SI units (e.g., Delbó et al. 2007, and updates from the first author), and components of the known asteroid pairs are typically in the kilometer-size range, we neglect the seasonal variant of the Yarkovsky effect, retaining only its diurnal variant. This is well justified because the seasonal part would typically produce an effect that is an order of magnitude smaller than the diurnal part (see, e.g., Bottke et al. 2006; Vokrouhlický et al. 2015). Additionally, the large size of bodies¹² implies that we may simplify rather involved radial-structure functions in the solution of Vokrouhlický (1998), replacing them with much simpler formulas.

In this approximation, the thermal acceleration \mathbf{f}_Y may be expressed as

$$\mathbf{f}_Y = \kappa[(\mathbf{n} \cdot \mathbf{s})\mathbf{s} + \gamma_1(\mathbf{n} \times \mathbf{s}) + \gamma_2 \mathbf{s} \times (\mathbf{n} \times \mathbf{s})], \quad (2)$$

where $\mathbf{n} = \mathbf{r}/r$ is the heliocentric unit position vector of the asteroid and \mathbf{s} is the unit vector of its spin axis. (For the sake of completeness, we provide in the Appendix a formulation of the seasonal component of the thermal accelerations, which would be needed in the cases of very high thermal inertia). The

magnitude of the acceleration and the weighting functions of each of the three terms in the brackets at the right hand side of Equation (2) read

$$\kappa = \frac{4\alpha}{9} \frac{SF}{mc}, \quad (3)$$

$$\gamma_1 = -\frac{1}{2} \frac{\Theta}{1 + \Theta + \frac{1}{2}\Theta^2}, \quad (4)$$

$$\gamma_2 = \frac{1 + \frac{1}{2}\Theta}{1 + \Theta + \frac{1}{2}\Theta^2}, \quad (5)$$

with $\alpha = 1 - A$, A is the Bond albedo, $S = \pi R^2$ is the cross-section in the spherical approximation, R is the radius of the asteroid, F is the solar radiation at the asteroid's distance r from the Sun, m is the asteroid mass, and c is the light velocity. The fundamental strength of the thermal effect is given by the thermal parameter $\Theta = \Gamma\sqrt{\omega}/(\epsilon\sigma T_\star^3)$, where Γ is the surface thermal inertia, ω is the rotation rate, ϵ is thermal emissivity, σ is the Stefan–Boltzmann constant, and T_\star is the subsolar temperature. The latter is given by $4\epsilon\sigma T_\star^4 = \alpha F$; as a result, T_\star is also a function of the heliocentric distance r . As a rule of thumb, the value of Θ is in the range of $\simeq 0.1$ –10. The last two terms in (2), weighted by the γ functions, represent the diurnal variant of the Yarkovsky effect, with the particularly important second term ($\propto \gamma_1$). This is because only this term results in a non-zero secular change $\langle da/dt \rangle$ of the orbital semimajor axis for circular orbits, therefore representing its leading effect. The third term provides a correction to the zero-eccentricity estimate of $\langle da/dt \rangle$ that is, however, only of the second order in e and consequently rather small. Nevertheless, it also results in short-period orbital perturbations, some of which may have an amplitude comparable to the estimated radius of the Hill sphere of the parent body of the 6070–54827 pair. Therefore, they are significant for the analysis of the past convergence of both orbits and in principle must be included in our integrations.

The first term on the right hand side of Equation (2) provides a zero $\langle da/dt \rangle$ value even for eccentric orbits. However, it only represents a zero-approximation of the seasonal variant of the Yarkovsky effect in the limit of very small thermal inertia. Indeed, if $\Theta \rightarrow 0$, we obtain $\mathbf{f}_Y \simeq \kappa \mathbf{n}$, simply the pressure of the reflected radiation. In the opposite limit of extremely large

¹² Note that the relevant thermal length-scale is given by the penetration depth of the diurnal wave, which, for typical surface inertia values and asteroid rotation rates, is a couple of decimeters at maximum.

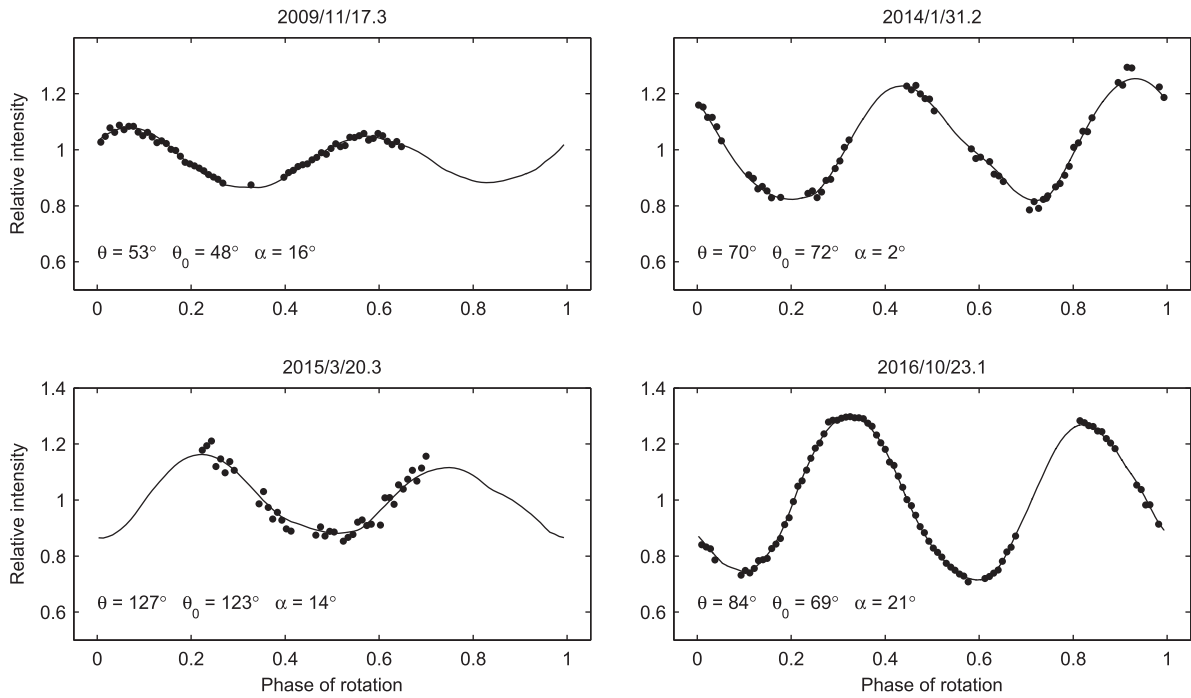


Figure 3. Sample of (54827) 2001 NQ8’s photometric data (symbols) fitted with synthetic light curves based on the convex shape model (solid line). We used the formally best-fit model with P2 pole orientation $(\lambda, \beta) = (242^\circ, -46^\circ)$ in ecliptic longitude and latitude, and sidereal rotation period $P = 5.877185$ hr. The viewing and illumination geometry is given by the aspect angle θ , the solar aspect angle θ_0 , and the solar phase angle α .

thermal inertia, i.e., $\Theta \rightarrow \infty$, the last two terms in (2) become zero and the first term would need to be changed to express more appropriately the seasonal variant of the Yarkovsky effect (e.g., Vokrouhlický & Farinella 1999, and the Appendix). Obviously, its complete representation already results in a non-zero $\langle da/dt \rangle$ value. At this moment, we do not include the seasonal variant of the Yarkovsky effect in our simulations mainly because the Θ parameter remains sufficiently small.

For sake of completeness of our formulation, we also include the effect of the direct solar radiation pressure in the simplest, spherical model

$$\mathbf{f}_{\text{SRP}} = \kappa' \mathbf{n}, \quad (6)$$

where

$$\kappa' = \left(1 + \frac{4}{9}A\right) \frac{\text{SF}}{mc}. \quad (7)$$

This is mainly to describe consistently the $\Theta \simeq 0$ limit in our approach. Otherwise, radiation pressure (6) produces only short-periodic effects of limited amplitude. More involved modeling of the radiation effects (see, e.g., Vokrouhlický & Milani 2000; Žižka & Vokrouhlický 2011) is not needed at this moment.

The fact that we have fairly good knowledge of s for both components in the pair does not imply that we should not observe the related uncertainties and use them in our solution. Thus each of the asteroid clones described above is given some initial value of s according to the uncertainty intervals from Sections 3.1 and 3.2. The uncertainty in rotational frequencies is insignificant for the Yarkovsky effect modeling and we take just the nominal values. In the same way, uncertainty in the Bond albedo is also not important, and we consider $A = 0.1$ for all clones. We also use the inferred emissivity $\epsilon = 0.9$. There

remain two more sources of uncertainty in the thermal accelerations model that we have to take into account (1) the value of the surface thermal inertia Γ and (2) the value of mass m , or bulk density ρ , of the asteroids. The former may be further constrained by observations in the thermal waveband, if they become available in the future. At this moment, we rely on statistical properties derived by Delbó et al. (2007) for the population of small, mostly near-Earth asteroids. The median value for asteroids of a few kilometers in size is $\simeq 200$ in SI units, and a standard deviation $\simeq 70$ in SI units. While approximate, these values are the best guess we can make. It is more difficult to make a bulk density estimate. Here we use information compiled by Carry (2012) for Sq-type asteroids, appropriate for our pair. This implies a median value $\simeq 2.3 \text{ g cm}^{-3}$ and a standard deviation $\simeq 0.3 \text{ g cm}^{-3}$. Note that we took a slightly smaller median value to reflect the small size of asteroids in the 6070 and 54827 pair.

Figure 5 shows the expected values of the secular semimajor axis drift $\langle da/dt \rangle$ for both asteroids as a function of their surface thermal inertia Γ . Obviously, the larger primary component (6070) Rheinland has about twice as small an intrinsic $\langle da/dt \rangle$ value (compare the solid red and dashed blue lines). However, the primary’s obliquity of nearly 180° helps in maximizing the Yarkovsky effect for its given size, while the smaller secondary has an obliquity of only $\simeq 138^\circ$. As a result, the expected $\langle da/dt \rangle$ are nearly comparable for both asteroids (see the solid red and blue lines). Given short rotation period values, the Yarkovsky effect is maximum for moderately small thermal inertia (the lower end of the expected value from the Gaussian distribution shown at the top of the figure) and becomes about half of the maximum expected value. It may also be noted that for the thermal inertia larger than $\simeq 500$, one would also need to include the seasonal component of the Yarkovsky effect. This is because in this range of high thermal inertia values the

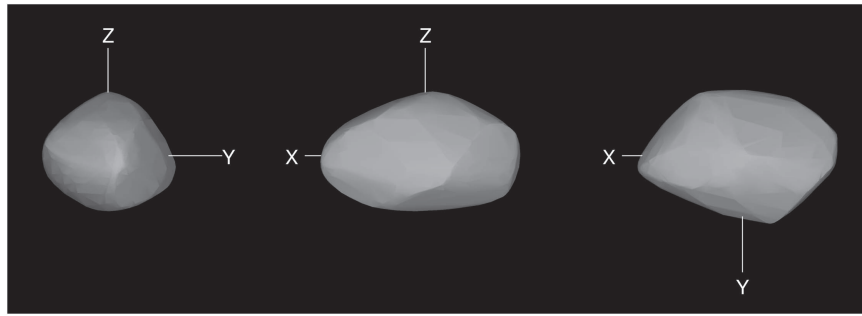


Figure 4. Shape model for (54827) 2001 NQ8 from the light-curve inversion analysis. We show the formally best-fit P2 model, but the model for P1 is basically identical. The three views are from the equatorial level (left and center) and the pole-on (right).

seasonal component contribution to $\langle da/dt \rangle$ would exceed 25% of the total effect.

In our simulations described below, every one of the clones is given a slightly different realization of the Yarkovsky parameters, all compatible with current observations. This replaces what Vokrouhlický & Nesvorný (2008), and following works, called the Yarkovsky clones.

4.2. New Features of the Model: Spin Axis Evolution

Thermal acceleration (2) depends on the direction of the spin axis s . The crudest approximation would assume that s is constant in the inertial space. However, since asteroids are never exactly spherical (e.g., Figure 4), the torque due to solar gravity makes s evolve. Importantly enough, a characteristic timescale of this precession motion is comparable, or even sometimes shorter, than the age of the pair (the relevant order of magnitude of the precession frequency is given by p in Equation (9)). Thus, in principle, dynamical evolution of s should be taken into account together with orbit propagation. Additionally, it is quite interesting to know the mutual orientation of spin vectors of the primary and secondary components at the moment of the pair formation. Astronomical observations provide this information at the current epoch, but in order to know the initial value one has to dispose of the spin propagator.

Luckily, this could be achieved at a rather low computational expense. Low-amplitude and short-period effects in s are of no importance for us, so we may afford to include just the simplest secular model. Assuming rotation about the shortest axis of the inertia tensor, we have (see, e.g., Colombo 1966)

$$\frac{ds}{dt} = p(N \cdot s)(N \times s), \quad (8)$$

where the precession constant p reads

$$p = \frac{3}{2} \frac{n^2}{\omega} \Delta. \quad (9)$$

Here, n is orbital mean motion, ω is rotational frequency that is constant in this model, and Δ is the dynamical ellipticity (Section 3.1). Finally, $N = (\mathbf{r} \times \mathbf{v})/|\mathbf{r} \times \mathbf{v}|$ is vector normal to the orbital plane directed along the orbital angular momentum (\mathbf{r} and \mathbf{v} are asteroid's heliocentric position and velocity). Should N be constant, Equation (8) would admit a trivial analytic solution expressing simple regular precession about this direction with frequency $p(N \cdot s)$. However, things are more complicated. Not only is the relevant timescale of spin precession comparable or shorter than the typical age of asteroid

pairs, motivating the use of (8), but it is also often comparable to the timescale with which N itself precesses in the inertial space due to planetary perturbations. Time-dependence of N makes Equation (8) complicated. Its analytical solution is possible only in the simplest case, called the Colombo top model, when the orbital inclination is constant and nodes precess uniformly in time (e.g., Colombo 1966; Henrard & Murigande 1987). In the real cases though, the spin evolution s must be determined numerically by integration of Equation (8). To that end, Breiter et al. (2005) developed an efficient symplectic integrator. Luckily their scheme is easy to accommodate in the orbit integration as described below.

Making the spin-axis integrator run, one has to specify the precession constant, the single parameter on the right hand side of Equation (8). In principle, p only depends on known parameters, namely the rotation frequency ω and dynamical ellipticity Δ . Of these two, however, the former is known much more accurately. For the purpose of our simulations, we only assume nominal values of the rotation frequency for 6070 and 54827, neglecting their small uncertainty. The story is different in the case of Δ . In principle, our shape models from Sections 3.1 and 3.2 provide nominal values of the dynamical ellipticity of both components in our pair (assuming homogeneous density distribution). However, as already mentioned in Section 3.1, the convex shape models obtained by the light-curve inversion methods cannot provide Δ with an accuracy better than $\sim 20\%$. So we need to account for this uncertainty. Therefore, each of the clones introduced above is assigned a Δ value chosen randomly from a Gaussian distribution with a mean equal to the nominal value and standard deviation of 20% of its value.

For the sake of reference, we note that the precession constant p for both components in the Rheinland and 2001 NQ8 pair is roughly $(20\text{--}25) \text{ arcsec yr}^{-1}$. This implies a precession period for (54827) 2001 NQ8 of about 50–65 kyr. Because the age of this pair is $\simeq 16$ kyr (Section 5), the spin axis of the smaller component in the pair changed in ecliptic longitude by some $90^\circ\text{--}110^\circ$, less than a complete revolution in the inertial space.

4.3. New Features of the Model: Implementation

Our fundamental numerical tool is a well-tested software package `swift`¹³ that we modified in two ways. First, we extended the orbital momenta perturbation within the implemented second-order leapfrog method in `swift` (see Sections 6 and 7

¹³ <http://www.boulder.swri.edu/~hal/swift.html>

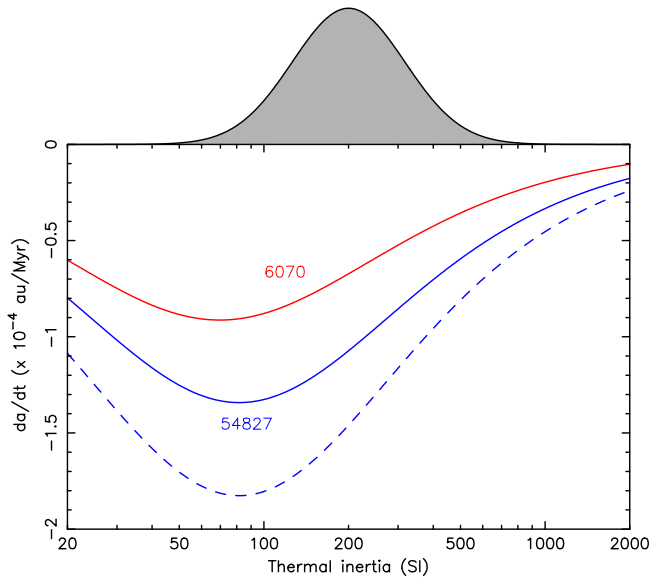


Figure 5. Secular value of the semimajor axis drift (da/dt) due to the Yarkovsky effect for both asteroids in the Rheinland and 2001 NQ8 pair. Nominal spin orientation from Sections 3.1 and 3.2 for both components is used. Red curve for the primary component (6070) Rheinland, blue curve for the secondary component (54827) 2001 NQ8; dashed blue would be the maximum possible (da/dt) value for 180° obliquity for reference. The gray Gaussian at the top shows the assumed distribution of the thermal inertia of both asteroids in our integrations.

of Wisdom & Holman 1991) to include the radiative accelerations. Therefore, in an elementary timestep dt (we used $dt = 1$ day or smaller) of the asteroid’s orbital integration we added thermal accelerations (2) and radiation pressure (6) to the gravitational perturbations from planets. Thanks to the low values of these radiative accelerations such a simple implementation has been successfully used and tested against analytic predictions in many previous works from our team. It is also similar to implementations of non-gravitational effects by other authors (see, e.g., Cordeiro et al. 1996).

The spin evolution for each of the clones is a new feature, missing in the original version of `swift`. Therefore, we programmed an entirely new level into the `swift` code that performs integration of Equation (8). We used the scheme presented by Breiter et al. (2005). Because the evolution of s is slow (secular), we may afford a much longer timestep dt' in solving (8). In practice we used $dt' = 10$ years, and for simplicity assumed orientation of s constant within each of the timesteps dt' . We believe this produces negligible effects on the orbit evolution. Note that the information about N , normal to the osculating orbital plane, is available online from the orbit integration in `swift`.

A particular problem we need to resolve in determining the asteroid-pair age is how to perform integration backward in time. With this in mind, we note that equations of orbital and rotational motion for heliocentric position \mathbf{r} and velocity \mathbf{v} , and the spin vector \mathbf{s} , are invariant under a transformation: $(\mathbf{r}, \mathbf{v}, \mathbf{s}; \kappa, \gamma_1, \gamma_2, p; t) \rightarrow (\mathbf{r}, -\mathbf{v}, -\mathbf{s}; \kappa, -\gamma_1, \gamma_2, p; -t)$. This includes time reversal, and also hints to us about the necessary transformation of each of the dynamical state vectors $(\mathbf{r}, \mathbf{v}, \mathbf{s})$ and force and torque-model parameters $(\kappa, \gamma_1, \gamma_2, p)$. As to the first, we simply revert velocities and spin vectors at the initial time. As to the second, we need to change the sign of the γ_1 parameter in performing the simulation into the past.

5. Results

Our nominal integrations used 5000 clones for both asteroids (6070) Rheinland and (54827) 2001 NQ8. We generated the initial orbits of these clone variants using the procedure outlined in Equation (1). Each of the clones has been given physical parameters needed for modeling the fine dynamical effects discussed in Sections 4.1 and 4.2. These included (indexes 1 and 2 are for the primary and secondary components in our pair of asteroids)

1. size estimates D_1 and D_2 from Sections 2.1 and 2.2 (including their uncertainty);
2. initial spin orientations s_1 and s_2 from Sections 3.1 and 3.2 (including their uncertainty);
3. surface thermal inertia Γ_1 and Γ_2 for both components; following results in Delbó et al. (2007), updated in Delbó et al. (2015), we used a lognormal distribution with a peak value of 200 and a standard deviation equivalent to 70 (both in SI units);
4. bulk densities ρ_1 and ρ_2 assumed to have Gaussian normal distribution with a mean value of 2.3 g cm^{-3} and a standard deviation of 0.3 g cm^{-3} , conforming to data reported in reviews of Carry (2012) and Scheeres et al. (2015);
5. dynamical ellipticity values Δ_1 and Δ_2 having Gaussian normal distribution with a mean value of the nominal solution from Sections 2.1 and 2.2 and 20% relative uncertainty.

Note that s_1 has been found very close to the south ecliptic pole, having just a single solution shown in Figure 1. On the contrary, the solution of s_2 has two equivalent possibilities P1 and P2 (see Section 3.2 and Figure 2). We thus conducted two sets of simulations starting s_2 from the uncertainty region of P1 and P2 separately. However, we found that results for both P1 and P2 are very similar and neither of the pole solutions could lead to better or worse past convergence of the orbits in this pair. We thus only report results for P1.

The integration timestep was $dt = 0.25$ days for orbit propagation of the clones and $dt' = 10$ years for the spin propagation. For simplicity, in between the timesteps of the spin propagation both s_1 and s_2 were assumed constant when used to evaluate the thermal accelerations (2). In the course of the orbital propagation of the clone clouds, we checked their relative configuration every 0.01 years. This means at each of these timesteps we considered all 2.5×10^7 pair realizations by comparing heliocentric Cartesian coordinates and velocities of all clones of (6070) Rheinland versus all clones of (54827) 2001 NQ8, and we evaluated their (1) mutual distance and (2) relative velocity. We recorded configurations for which the distance was smaller than the estimated Hill radius of the parent body and the relative velocity smaller than its escape velocity (see Section 2.2).

5.1. Convergence at the Nominally Adopted Age

Vokrouhlický & Nesvorný (2008) were the first to note the convergence of (6070) Rheinland and (54827) 2001 NQ8 at a very close distance in Cartesian space some 17 kyr ago, interpreting this event as the physical origin of the two asteroids from a fission of their common parent body. Vokrouhlický & Nesvorný (2009), and later Vokrouhlický et al. (2011) and Galád (2012), substantiated this solution by

accounting for more details in the propagation model, such as mutual gravitational attraction of the two components during the short time interval in which they initially separated. In all of these publications, $\simeq 17$ kyr remained to be the nominally adopted age of the pair. In this section, we follow this analysis and first focus of the mutual configuration of the orbits of (6070) Rheinland and (54827) 2001 NQ8 in the past 20 kyr. In the next section, we explore their orbit evolution in a more distant past.

Figure 6 shows the statistical age-distribution of the successfully converging solutions, namely the number of pair identifications that approached at a distance of the Hill radius of the parent body at small relative velocity (for simplicity, we round the values to 900 km and 2.5 m s^{-1} , Section 2.2). We note that the successful trials are localized into a rather tight interval of ages between 16.15 and 16.48 kyr. During the first hundred years, i.e., 16.15 to 16.25 kyr only a small number of encounters were recorded, such that the predominant interval during which a significant number of encounters occur is 16.25 and 16.45 kyr (see also Figure 11). Taken straight, we could match the distribution with Gaussian having a mean value of 16.34 kyr and a standard deviation of 0.04 kyr. This would largely supersede previous solutions from Vokrouhlický & Nesvorný (2009) or Vokrouhlický et al. (2011), in which the formal uncertainty of the age solution was about three to five times larger. To some extent, this is expected since a simultaneous constraint of the rotation pole orientation for both components in the pair should result in a more accurate modeling of the thermal accelerations. Formally, the best-converging couples of clones appeared to encounter at $\simeq 1$ km distance, which is already less than the sum of the asteroids' radii, and had a relative velocity between 0.1 – 0.2 m s^{-1} . The latter is also quite smaller than the estimated escape velocity $\simeq 2.5 \text{ m s}^{-1}$ from the parent body of the pair (Section 2.2).

At the best performance, nearly 33,000 of the 2.5×10^7 clone-identification trials at each timestep were successful. Fractionally, this is 0.13% of all tested cases. It would be interesting to check that this is about the expected success rate, an issue that was so far neglected in the pair-convergence studies. In order to shed light on this topic, we recall that the clones are initially localized in a very tight region of space, roughly ellipsoidal in shape (see Section 4). However, this zone quickly expands due to various effects. During the initial tens of thousands of years, the clone divergence is governed basically by two effects, both in the along-track direction: (1) Keplerian shear due to their slightly different mean values of the semimajor axis and (2) the cumulative effect of a change in the semimajor axis due to the Yarkovsky effect. By numerically tracking maximum distance between clones of each of the asteroids, we found that (2) dominates. Its effect can be well approximated by formula (29) in Vokrouhlický et al. (2000), where the Yarkovsky drift rate $\langle da/dt \rangle \simeq 6 \times 10^{-5} \text{ au Myr}^{-1}$ is the maximum difference of its value for different clones. The longest axis of the ellipsoidal zone occupied by clones, only $\simeq 450$ km initially, becomes $\sim 0.01 T^2$ kilometers in T years. At $T \simeq 1.6 \times 10^4$ this value grows to as much as 2.6×10^6 km. This covers an arc extending angularly $\simeq 0.4^\circ$ along the orbit, still a comfortably small section. While the along-track uncertainty expands quickly, the perpendicular directions remain much smaller, less than two orders of magnitude larger than their initial values of 100 km.

The above-estimated distance of clones in the clouds is the maximum possible. We found that the median distance from a clone to clone is quite smaller, certainly an expression of the fact that the difference in the Yarkovsky drifts is actually smaller. We found that the median distance between the clones at $\simeq 16$ kya is only about 3.2×10^5 km for (6070) Rheinland and about 5.6×10^5 km for (54827) 2001 NQ8. It is notable that the 900 km size Hill radius of the parent body represents fractionally about $\sim 900/(4.5 \times 10^5) \simeq 0.2\%$ of the characteristic clone distance in the along-track direction. This is very close to the success rate with which we found converging clone identifications at about 16.3 kya. There is only one possibility for this good correspondence: the ellipsoidal regions filled with the clones must be nearly perfectly aligned. In any other configuration, for which their long axes would be tilted away from each other, the success rate of convergence must have been smaller. We believe that this is not only a satisfactory explanation of the quantitative success in convergence, but it also strengthens the case of 16 kyr age of this pair.

Further evidence for perfect alignment of clone ellipsoids is provided by Figure 7, in which we show normalized cumulative distribution $N(d)$ of converging clone distances d . As mentioned above, the best achieved d values are as small as $\simeq 1$ km. Interestingly, except for the smallest distances $d \leq 150$ km, $N(d)$ is basically linear with d . This is expected for randomly distributed points in a one-dimensional space. Such a result indicates that the role of dimensions (directions) perpendicular to the long axis of the uncertainty ellipsoid of clones is small.

However, we should not overstate our result. First, when the clones encounter at a distance of a few Hill radii of their parent body, i.e., 1000–3000 km, their mutual gravitational attraction must influence their trajectories (see, e.g., Vokrouhlický & Nesvorný 2009). This effect has been neglected here for simplicity. In principle, this additional interaction may result in more cases converging, perhaps extending slightly from the formal uncertainty of the age-distribution while not affecting the mean value (Figure 6). More importantly, our tests have shown that the gravitational perturbations from the minor bodies included in our simulation, Ceres, Pallas, and Vesta, are indeed non-negligible (see conclusions in Galád 2012). If these bodies are excluded, the age estimate would shift by as much as 600–800 years toward older ages as seen, e.g., in solutions of Vokrouhlický & Nesvorný (2009) or Vokrouhlický et al. (2011). Luckily, these three largest bodies in the main belt represent compositely more than 50% of its mass, but it is conceivable that the gravitational effects of the remaining bodies in the main belt would also have a non-negligible effect on the age solution of the pair Rheinland and 2001 NQ8. Analysis of these perturbations is, however, beyond the scope of the present paper.

The ability to track not only the orbital motion of the asteroid clones, but also their spin evolution, is one of the benefits of our propagation model described in Section 4. In particular, we are interested in the mutual spin orientation of the primary (s_1) and secondary (s_2) clones at the moment of their convergence, i.e., the close approach in the past epochs. This is because we know that the spin axis orientation evolves and the currently observed values reported in Sections 3.1 and 3.2 may not inform us correctly about the mutual configuration of s_1 and s_2 at the origin of the pair. Figure 8 shows the needed information, namely the recorded values of the angle β between s_1 and s_2 at the moment of convergence for all converging clone pairs in

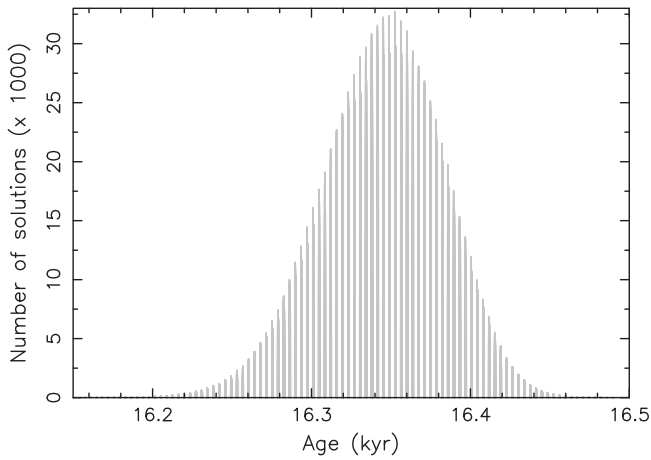


Figure 6. Number of converging pair identifications among 5000 clones of (6070) Rheinland and 5000 clones of (54827) 2001 NQ8. Trial identifications were performed every 0.01 years, and the bar graph shows data in each timestep. At the optimum bin, more than 0.1% of trials converged. Note the blank steps, with no converging cases. This is because the convergence repeats roughly once in a revolution period at a certain orbital configuration (see also Figure 11).

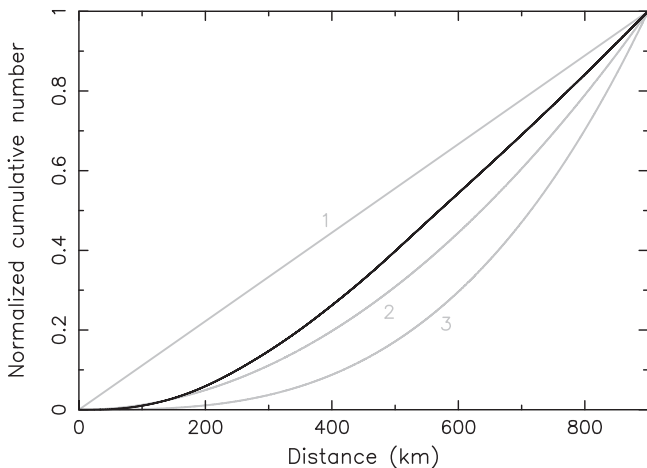


Figure 7. Normalized cumulative distribution of the distances d between the converging clones of Rheinland and 2001 NQ8 (i.e., $d \leq 900$ km). The best cases have $d \simeq 1$ km, but these are statistically rare; many more clone pairs have distances of several hundreds of kilometers. The gray curves correspond to power laws $N(d) = (d/900)^\alpha$, for three values $\alpha = 1, 2,$ and 3 (labels).

our simulation. Distribution of β values, adjoined to the right ordinate, has a mean value of 38° and a standard deviation of 12° . While there exists a tail of solutions that would have $\beta \leq 20^\circ$, these represent only a small fraction of all possibilities. There is also a slight correlation between β and age, such that the smaller β values occur for older ages (correlation coefficient of $\simeq -0.54$, see Bertotti et al. 2003).

Overall, we conclude that the initial angular separation of s_1 and s_2 at the moment of the pair origin was significant, most likely about 38° . Note, however, that our solution can provide only s_1 and s_2 at the moment when the two fragments from the parent body fully separated to large distance (formally to “infinity”). Even if the two components separate in the equatorial plane of the parent body with initially having spin close to parallel, the angular momentum exchange between the rotation and translational motion of the two asteroids can result in a final tilt between the s_1 and s_2 when the bodies eventually

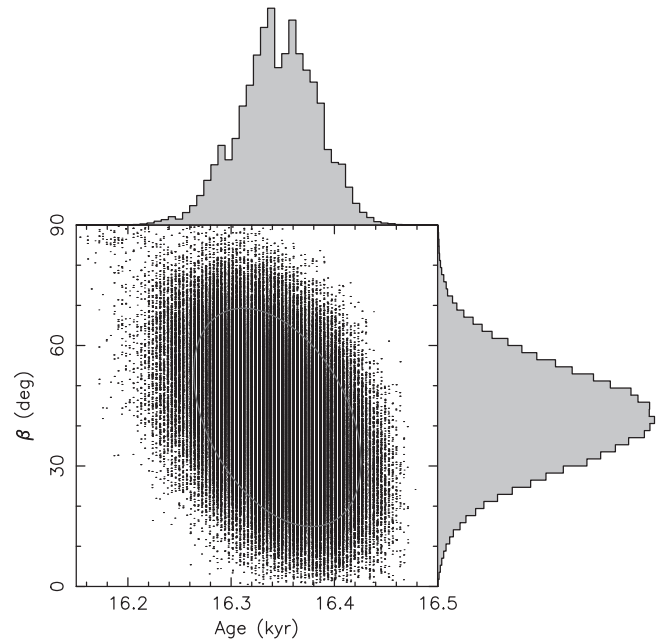


Figure 8. Angular separation β between pole orientations of the primary and secondary (ordinate) at the moment of convergence (abscissa). The gray histograms at the top and right show respective one-dimensional distributions of the age and β solutions. The gray ellipse shows the 90% confidence level region of the two-dimensional distribution of the β and age values (see Chap. 20 of Bertotti et al. 2003).

separate at a large distance. In fact, detailed data about asteroid pairs, such as those presented for the Rheinland and 2001 NQ8 couple in this paper, provide an interesting constraint for modelers of the separation mechanics.

In order to glean more details, we show in Figure 9 the dependence of the thermal inertia values Γ_1 and Γ_2 of the converging clones, for the primary and secondary, versus the time of separation. The correlation is rather weak (correlation coefficients ± 0.38). This indicates that thermal observations of either Rheinland or 2001 NQ8, while interesting by itself, would not have the capability to significantly increase the accuracy of the age solution for this pair. We investigated other parameters of the model and found that the initial obliquity of (54827) 2001 NQ8 seems to be the most strongly correlated with the age solution (correlation coefficient -0.7). This is shown in Figure 10. Therefore, it appears that continuing photometric observations of the secondary component in this pair, with the goal to tighten the uncertainty interval of the pole position, may help improve the age solution.

To understand the effects of massive asteroids included in our simulation, we also tracked in detail the minimum distance of the propagated asteroid clones for both Rheinland and 2001 NQ8 to Ceres, Pallas, and Vesta. In particular, at every timestep dt of our integration, we evaluated these distances. We found that there are only distant encounters to the massive perturbers in the past 20 kyr. The closest occurred for Vesta, about 8.85 kya, when some of the clones approached this large asteroid at about nine Hill radii: in quantitative terms, we found that 2% of clones of (6070) Rheinland underwent these approaches and more than an order of magnitude less for clones of (54827) 2001 NQ8. In both cases this is still a safe distance not to expect a violently chaotic perturbation to the clouds of clones. As a result, the overall effect of the massive asteroids in

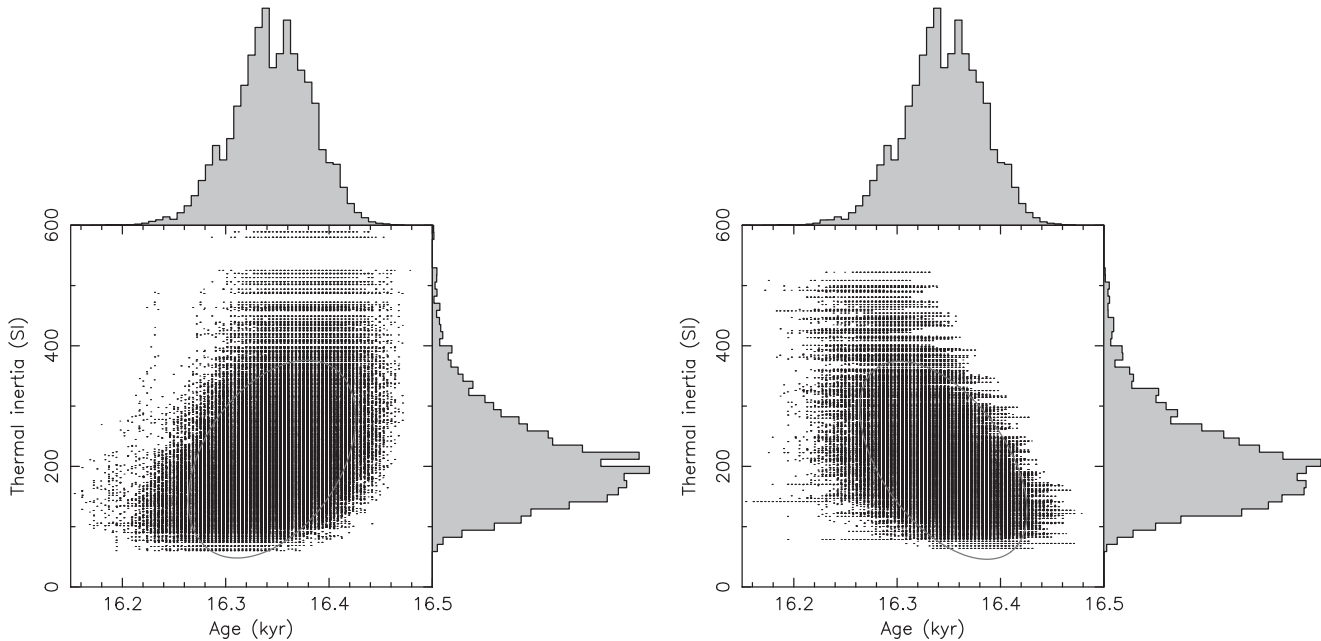


Figure 9. Surface thermal inertia of the primary (left panel) and the secondary (right panel) converging clones vs. age at the abscissa. The gray histograms at the top and right show respective one-dimensional distributions of the age and Γ values.

the last 20 kyr is just the secular effect on the clone mean motion.

5.2. Convergence Beyond the Nominally Adopted Age?

In the previous section, we followed the orbits of asteroid clones in the 6070–54827 pair until their very close approaches $\simeq 16.3$ kya and we identified this event with their origin. However, is this the true and only solution for the origin of this pair, or are there other possibilities more distant in time? This issue has not yet been thoroughly studied for most of the known pairs.

Is it even possible to expect more solutions for the origin of the 6070–54827 pair in the situation when a fairly robust convergence was already found? In principle yes. Consider the example of asteroids (1270) Datura and (215619) 2003 SQ168 discussed in Section 4 of Vokrouhlický & Nesvorný (2008). These two objects, members of the Datura family, resemble the configuration of an asteroid pair by having extremely similar orbits. Their very similar values of the longitude in orbit prompted authors in Vokrouhlický & Nesvorný (2008) to investigate a possibility of a very recent origin of these two bodies. However, by extending their backward orbital propagation to one megayear, they noticed that the very close approaches of the two bodies repeat once every ~ 150 kyr for the whole timespan of the simulation. They interpreted this effect as a synodic cycle in which the mean longitudes become similar. Obviously, its unusual length is given by the extremely similar values of the mean semimajor axis. Recently, Žižka et al. (2016) studied this effect in more detail when attempting to prove the very young age of the asteroid pair consisting of (87887) 2000 SS286 and (415992) 2002 AT49. However, the possibility of an older convergence solution for the pair (6070) Rheinland and (54827) 2001 NQ8 had not yet been analyzed. Given our solid constraint on the value of the Yarkovsky accelerations in both orbits, we pay some attention to this problem in this section.

The importance of the Yarkovsky effect constraint for our issue here is as follows. If there were only gravitational effects in the orbital evolution, the close alignment of the orbits after completing a synodic cycle would eventually be broken by a slow diffusion of the orbits. However, this process is very slow and could effectively preserve the proximity of the two orbits for millions of years. However, the thermal accelerations make the orbital semimajor axes change much faster. Therefore, conditions for close encounters of the two orbits could be prevented quite faster.

In order to understand the situation, we performed a second series of clone propagations into the past. Since now we set the maximum time to be 250 kyr, the computer time requirements are quite larger. To keep them reasonable, we used only 2000 clones for both (6070) Rheinland and (54827) 2001 NQ8 generated by the same procedure as above. We also used a longer timestep of $dt = 0.5$ day for orbit propagation and we checked the mutual clone configuration only every 0.05 years. We kept $dt' = 10$ years for the propagation of spin orientation of all clones.

Figure 11 shows the results. The left panels show the whole integrated timespan of 250 kyr: (1) the upper part gives the minimum recorded distance between the clones of (6070) Rheinland and the clones of (54827) 2001 NQ8 and (2) the lower part gives the relative velocity of these closest clone configurations. Note that the logarithmic scale on the ordinates, which allows us to show a large range of values. This is necessary because initially the relative distances and velocities are a couple astronomical units and tens of kilometers in second, as the clouds of clones of each of the bodies reside on very different longitudes along the common orbit. However, we also want to show the situation of convergence, when the relative distances are only kilometers to hundreds of kilometers and the mutual velocities are only centimeters per second. In particular, our quantitative criteria for convergence of the clones, namely their distances smaller than the Hill sphere of the parent body ($\simeq 900$ km) and mutual

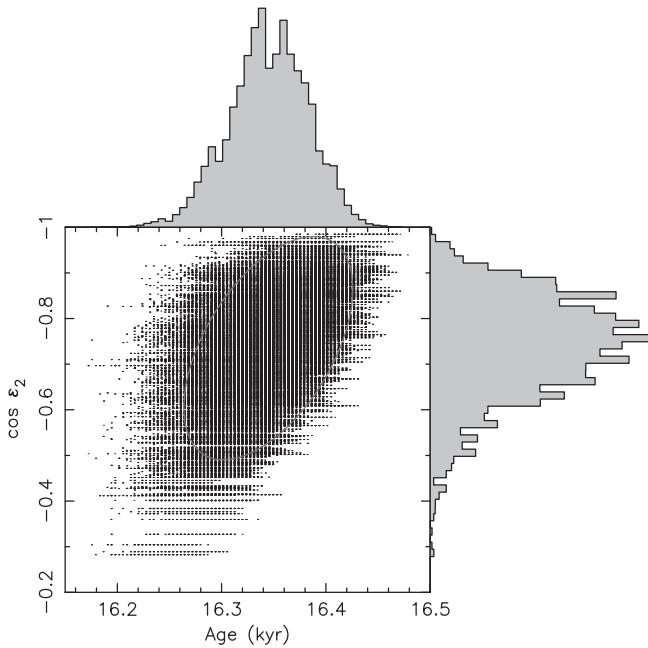


Figure 10. Cosine of the initial obliquity ε_2 of the secondary clones (ordinate) vs. age at the abscissa. The gray histograms at the top and right show respective one-dimensional distributions of the age and ε_2 values.

speed smaller than the escape velocity from the parent body ($\approx 2.5 \text{ m s}^{-1}$), are shown by gray lines. Focusing first on the first 20 kyr interval, studied in Section 5.1, we note how the mutual distances and relative velocities of the clones rapidly collapse to convergence at ≈ 16.05 kyr and expand to large distances and mutual speeds from each other at ≈ 16.45 kyr. A zoom on this period of time is given in the middle panels. The critical period of convergence is characterized by a nearly perfect overlap of the ellipsoidal zones in space where the clones of both asteroids are located. Because the two structures slowly slide relative to each other in time, there is initially less successful convergence identifications between the clones. This number increases to optimum at ≈ 16.3 kyr, and then again decreases (Figure 6). We estimated that at this epoch the cloud zones are still very small compared to the whole orbit circumference, the convergence possibility is shut and the two clouds diverge from each other. We also note that during the interval of time when convergence is achieved, the minimum clone distance oscillates from a value of less than 900 km to a value little more than 10,000 km. The rightmost panels provide the explanation: the period of these oscillations is equal to the orbital period of the clones. Planetary perturbations produce large-enough short-period perturbations of the clone locations, such that their clouds periodically pulsate from the overlapping configuration to the non-overlapping state. This implies that the convergence occurs at a particular phase of the revolution about the Sun.

Moving now to an epoch more distant in the past, we expect two effects. First, the region in space where the clones are located expands with time, eventually becoming extended over the whole orbit. The differential value of the Yarkovsky effect on clones of each of the components, though not huge (those of 6070 have a slightly smaller mean $\langle da/dt \rangle$ value than those of 54827; see Figure 5), makes the characteristic clone semimajor axis values different. Close-enough proximity of clones might still be achieved at the expense of different eccentricity values,

but in this case the relative speed of the clones would typically be large.

Data in Figure 11 confirm both conclusions. At about 50 kya the two clone clouds are still compact enough to perform their global encounter, i.e., their approach followed by their separation, but they miss each other at a minimum distance of $\approx 25,000$ km and do not offer the possibility for a successful convergence. Briefly, after the 50 kyr epoch in our integration, the clone clouds of (54827) 2001 NQ8, and shortly after those of (6070) Rheinland, undergo a close encounter with the dwarf planet (1) Ceres in our simulation¹⁴ (see Figure 12). Unlike in the case of encounter ≈ 8.85 kya, when only a small fraction of clones approached (4) Vesta at a large distance, now all clones of both components approach (1) Ceres at a very small distance. These events rapidly stretch the long axes of the clone ellipsoids, such that their length starts propagating in time significantly faster than before. This accelerated uncertainty in the location of clones shortens the synodic cycle effect, eventually erasing it entirely (at about 90 kyr; Figure 11). At that moment, the clones of (54827) 2001 NQ8 extend over all possible longitudes along the orbit. Mutual distances to the clones of (6070) Rheinland become limited to smaller values because, for each of its clones, there is one for 54827 that has an approximately similar longitude in orbit and pulsates in what remained from the synodic cycles. Importantly, the minimum relative speeds become gradually larger and larger, $\geq 10 \text{ m s}^{-1}$ for epochs beyond 100 kyr. This is because the close encounter clone conditions occur only at the expense of choosing slightly different eccentricity or inclination values. Such larger relative velocities can hardly be produced by a gentle process of the rotational split of the two components in the pair. The apparent possibility of near approaches beyond 250 kyr in the past, as shown by the results in Figure 11, is actually false. A close inspection reveals that the minima of relative velocities at the bottom panel of this figure are not aligned in phase with the minima of the relative distances at the top panel.

Returning to the Figure 12, one may note a number of interesting structures in the sequence of possible close encounters to the most massive bodies in the main belt. The principal features may be understood by the synodic (secular) cycle of nodal lines of the clones of either of the components in the 6070–54827 pair and one of the large bodies. For instance, the $\approx 14.3 \text{ arcsec yr}^{-1}$ difference in the proper s frequencies of Ceres and Rheinland corresponds to ≈ 91 kyr synodic nodal cycle. Obviously, when the longitude of nodes of the two orbits get close, there are more chances of close encounters. This is seen in the repetition pattern of encounters to Ceres in the left panels of Figure 12. The proper s frequencies of both Vesta, and especially Pallas, are closer to those of Rheinland’s orbit, so the synodic nodal cycle becomes ≈ 250 kyr and ≈ 860 kyr long for Vesta and Pallas. This also explains, together with quite higher inclination of the Pallas’ orbit, why the encounters with Pallas are less frequent (and thus less important).

While we do not have definitive proof, results from this experiment indicate that the nominal solution for the origin of the 6070–54827 pair at ≈ 16.3 kya is the only possibility over the analyzed timespan of 250 kyr. Attempts to search for older

¹⁴ We mention that many clones of the secondary (54827) 2001 NQ8 also underwent close encounters to (2) Pallas in between 21.34 and 21.44 kya (see the middle panel on Figure 12), but these have less effect because they occur at very high relative velocity due to Pallas’ large orbital inclination value.

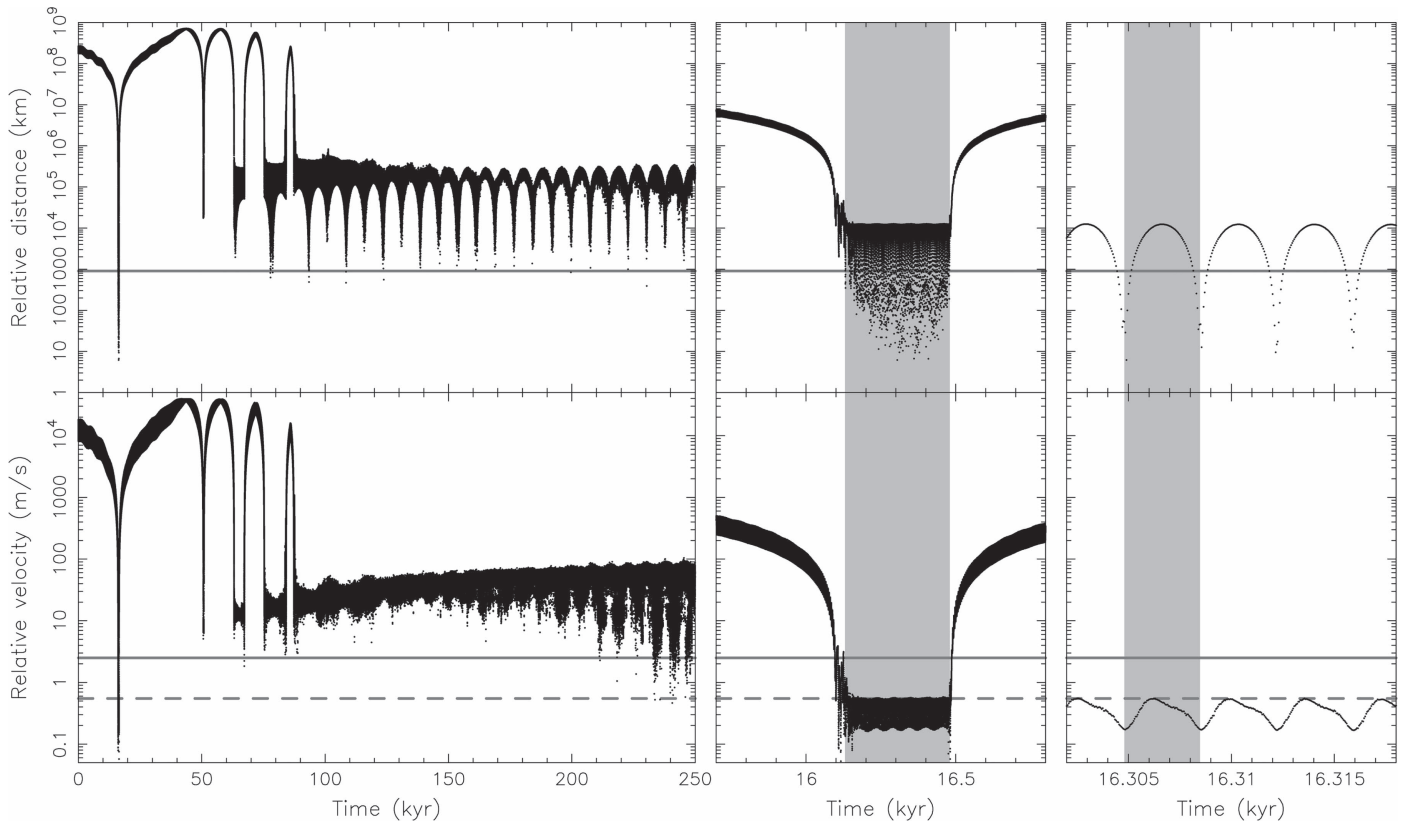


Figure 11. Top panels: minimum distance between clones of (6070) Rheinland and (54827) 2001 NQ8 as a function of time in the past. Each of the asteroids was represented by 2000 clones and at every 0.05 years, we consider all possible identifications between the clones of the primary and secondary. The gray horizontal line shows the reference distance of 900 km corresponding to the estimate Hill radius of the parent body of the pair. Bottom panels: relative velocity of the two closest clones for which their distance was shown in the top panel. The gray horizontal line shows the reference velocity 2.5 m s^{-1} corresponding to the escape speed from the parent body of the pair. The dashed line shows the maximum relative velocity of the closest clones in the nominal range of ages, i.e., between 16.15 to 16.45 kyr. Middle and right columns show zoom in time to (1) the interval 15.7 to 16.8 kyr, which includes the nominal age range discussed in Section 5.1 (gray interval), and (2) the very short timescale of 16 years that includes about 4.5 orbital revolutions about the Sun. The rightmost panels indicate that the convergence occurs only at a particular phase of the revolution cycle (the gray interval shows one revolution about the Sun).

alternatives would face problems due to the rapid divergence of the orbits both due to the thermal accelerations and gravitational perturbations from massive asteroids.

6. Discussion and Conclusion

One interesting problem related to the 6070–54827 pair has to do with a constraint on possible further objects along their orbit. In particular, one might want to know the maximum size of an undiscovered fragment (or fragments) from the formation event of this pair (assuming they exist). In order to, at least very roughly, tackle this issue, we selected the following heliocentric orbital zone: $a \in (2.3\text{--}2.5) \text{ au}$, $e \geq 0.15$, and $i \leq 7^\circ$, that very broadly encompasses orbits of Rheinland and 2001 NQ8 (all orbital elements are osculating in the MJD 57800.0 epoch, no limits on the secular angle and longitude in orbit). This means we did not perform any specific analysis related to the particular orbital configuration of this pair, but rather probed the general capability of current sky surveys to discover objects in approximately the same orbital zone. We found that (1) multi-opposition asteroids in this target zone discovered in the past five years have all but one absolute magnitude $H \geq 17.1$ (the exception being 2016 CJ148, which has a very uncertain orbit; A_{stdYs} gives $H \simeq 17.6$ for this object and rejects 2014 observations); and (2) there are some 140 single-opposition asteroids in the target zone with magnitudes between 14 and 17, mostly detected before 2012,

which have yet to be re-detected. However, there is only a handful of subsets that were detected in the last two years in this magnitude range and at least half of them are single-night tracterets. Therefore, some (or many) of them might result from detection noise or mistakes. While this issue would certainly need a more careful analysis in the future, it seems to us that it is unlikely that there are more objects with $H \leq 17$ (equivalent to $D \geq 1.2 \text{ km}$) accompanying asteroids (6070) Rheinland and (54827) 2001 NQ8 along their orbit.

Another important piece of information would be provided by a direct detection of the Yarkovsky effect in the orbit of (6070) Rheinland and/or (54827) 2001 NQ8. At first sight, such an idea seems odd because the Yarkovsky effect has been detected so far in the case of the best suited orbits of near-Earth asteroids (e.g., Vokrouhlický et al. 2015, and references therein). However, fast advances in very precise astrometry could make this goal realistic. For instance, the *Gaia* mission will collect sub-milliarcsecond astrometry for thousands of asteroids during its five-year lifetime cycle. This will allow a significant boost in detection of the Yarkovsky effect, including possibly some objects in the main belt (e.g., Delbó et al. 2008). Using formula (30) of Vokrouhlický et al. (2000), we estimate that in the nominal duration of the *Gaia* mission, the Yarkovsky effect would produce an angular quadratic advancement along the orbit of both asteroids of $\simeq 0.15$ milliarcseconds. Given modeling in Delbó et al. (2008), plus the update

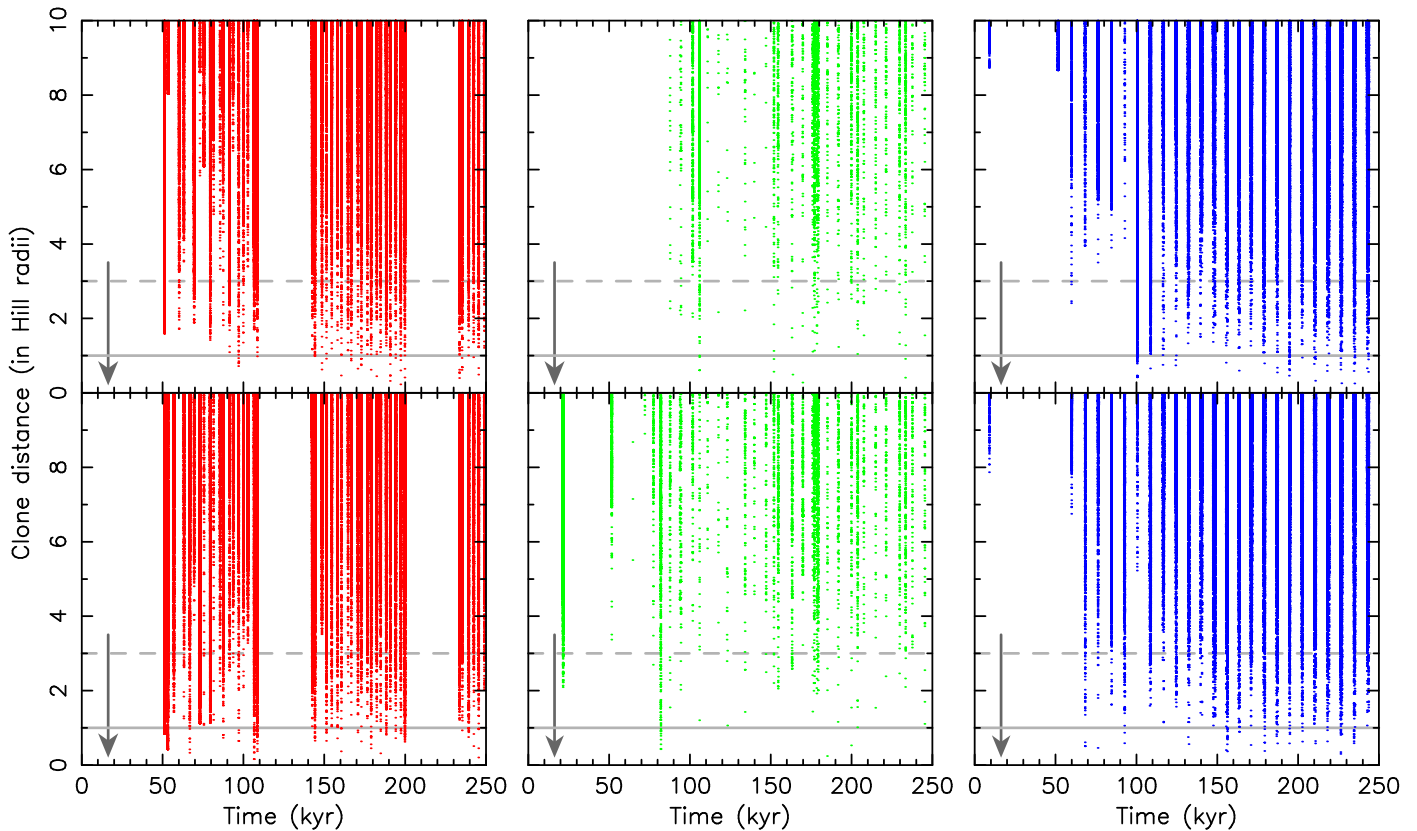


Figure 12. Close encounters to massive bodies in the main asteroid belt in our longer simulation: (1) clones of (6070) Rheinland at the top and (2) clones of (54827) 2001 NQ8 at the bottom. Left panels (red symbols) for encounters to the dwarf planet (1) Ceres, middle panels (green symbols) for encounters to (2) Pallas, and right panels (blue symbols) for encounters to (4) Vesta. Time at the abscissa in kyr, and distance to the massive body in terms of Hill radii of the body at the instantaneous heliocentric distance on the ordinate. The horizontal lines show a threshold of one Hill radius (solid line) and three Hill radii (dashed line). For reference, we note that the mean Hill radius of (1) Ceres is $\approx 220,000$ km, the mean Hill radius of (2) Pallas $\approx 195,000$ km, and the mean Hill radius of (4) Vesta is $\approx 125,000$ km. The arrows indicate the nominal age of ≈ 16.3 kyr.

on realistic performance of the spacecraft in Tanga et al. (2016), the direct Yarkovsky detection for (6070) Rheinland or (54827) 2001 NQ8 from *Gaia* data solely does not seem very promising. However, we may mention that a combination of the *Gaia* data with astrometry from a hypothetical mission having about the same performance undertaken a decade after *Gaia*'s mission termination, would reveal the needed signal.

Apart from the formulation of a new propagation scheme, applicable to the best characterized asteroid pairs, the main novel result in this paper concerns relative spin orientation of the two components in the 6070–54827 pair at the moment of their separation. While confirming the same sense of their rotation, as in the case of the much older pair (2110) Moore-Sitterly and (44612) 1999 RP27 (Polishook 2014), we also showed that the spin orientation of Rheinland and 2001 NQ8 was not collinear. The obtained tilt of $38^\circ \pm 12^\circ$ is statistically significant and needs to be elucidated by a detailed modeling of the fission process and the brief phase in which the components of the proto-pair separated to at least the Hill radius distance from each other. It would be very interesting to increase the sample of asteroid pairs for which we would be able to resolve the mutual orientation of their spin vectors, ideally at the moment of their separation. Note that the latter requires not only data from current photometric observations, but also a reliable orbit and spin propagation to the past. The pair of asteroids Rheinland and 2001 NQ8 is unique in this respect so far, because of their very young age and large size. Most commonly, the pairs are young, but have at least one

component that is very small, and thus are difficult to photometrically observe; or their age is large, and thus necessarily uncertain.

We thank David Polishook whose numerous comments helped to improve the original version of this paper. This research was supported by the Czech Science Foundation (grants GA17-00774S and GA13-01308S). This work was based on data collected with the Danish 1.54 m telescope at the ESO La Silla Observatory within the NEOSource project. The observations of (6070) Rheinland were partially taken with the 0.77 m telescope at La Hita observatory, which is jointly operated by the Instituto de Astrofísica de Andalucía-CSIC and Fundación Astrohita. Operations at Sugarloaf Mt. Observatory were supported by a Gene Shoemaker NEO grant from the Planetary Society. The work at Abasumani was supported by the Shota Rustaveli National Science Foundation, Grant FR/379/6-300/14.

Appendix Seasonal Component of the Yarkovsky Effect

In this Appendix, we briefly outline how the seasonal component of the Yarkovsky effect may be included in the propagation model at the lowest order. The formulation follows the linearized model developed in Vokrouhlický & Farinella (1999) and also used in Vokrouhlický et al. (2000). Most of the notation remains the same as in Sections 4.1 and 4.2.

For large-enough surface inertia, one may want to include both components of the Yarkovsky effect. The last two terms in the right hand side of Equation (2) account for the diurnal variant, but the first term in the same equation is just a “dummy” expression of the seasonal part of the Yarkovsky effect. If one wants to include the correct form of the seasonal effect, at least to the zero order in eccentricity of the heliocentric orbit, it is necessary to replace the first term in the right hand side of Equation (2) with the following formula

$$\vec{f}_Y = \kappa [\bar{\gamma}_2 (\mathbf{n} \cdot \mathbf{s}) + \bar{\gamma}_1 (\mathbf{N} \times \mathbf{n}) \cdot \mathbf{s}] \mathbf{s}, \quad (10)$$

where functions

$$\bar{\gamma}_1 = -\frac{1}{2} \frac{\bar{\Theta}}{1 + \bar{\Theta} + \frac{1}{2}\bar{\Theta}^2}, \quad (11)$$

$$\bar{\gamma}_2 = \frac{1 + \frac{1}{2}\bar{\Theta}}{1 + \bar{\Theta} + \frac{1}{2}\bar{\Theta}^2} \quad (12)$$

have the same form as before (Equations (4) and (5)), except the diurnal thermal parameter Θ becomes now replaced with its seasonal counterpart $\bar{\Theta} = \Gamma \sqrt{n} / (\epsilon \sigma T_\star^3)$. Note the only difference consists in the rotation frequency ω being replaced with the orbital mean motion n . Because $\bar{\Theta}/\Theta = \sqrt{n}/\omega \ll 1$, the zero order approximation is considering $\bar{\Theta} \simeq 0$. In this limit, Equation (10) provides $\vec{f}_Y \simeq \kappa (\mathbf{n} \cdot \mathbf{s}) \mathbf{s}$, the approximation used in the first term of Equation (2). At this level, though, there is no secular effect on the orbital semimajor axis. Out of the two terms in the right hand side of Equation (10), it is the second term that leads to what is generally called the seasonal Yarkovsky effect.

References

- Bertotti, B., Farinella, P., & Vokrouhlický, D. 2003, *Physics of the Solar System—Dynamics and Evolution, Space Physics, and Spacetime Structure* (Dordrecht: Kluwer)
- Bottke, W. F., Vokrouhlický, D., Rubincam, D. P., & Nesvorný, D. 2006, *AREPS*, 34, 157
- Breiter, S., Nesvorný, D., & Vokrouhlický, D. 2005, *AJ*, 130, 1267
- Carruba, V., Nesvorný, D., & Vokrouhlický, D. 2016, *AJ*, 151, 164
- Carry, B. 2012, *P&SS*, 73, 98
- Chesley, S. R., Farnocchia, D., Nolan, M. C., et al. 2014, *Icar*, 235, 5
- Chesley, S. R., Ostro, S. J., Vokrouhlický, D., et al. 2003, *Sci*, 302, 1739
- Colombo, G. 1966, *AJ*, 71, 891
- Cordeiro, R. R., Gomes, R. S., & Vieira Martins, R. 1996, *CeMDA*, 65, 407
- Delbó, M., Dell’Oro, A., Harris, A. W., Mottola, S., & Mueller, M. 2007, *Icar*, 190, 236
- Delbó, M., Mueller, M., Emery, J. P., Rozitis, B., & Capria, M. T. 2015, in *Asteroids IV*, ed. P. Michel, F. E. DeMeo, & W. F. Bottke (Tucson, AZ: Univ. Arizona Press), 107
- Delbó, M., Tanga, P., & Mignard, F. 2008, *P&SS*, 56, 1823
- Dobrovolskis, A. R. 1996, *Icar*, 124, 698
- Đurech, J., Sidorin, V., & Kaasalainen, M. 2010, *A&A*, 513, A46
- Erikson, A., Mottola, S., Lagerros, J. S. V., et al. 2000, *Icar*, 147, 487
- Farnocchia, D., Chesley, S. R., Vokrouhlický, D., et al. 2013, *Icar*, 224, 1
- Galád, A. 2012, *A&A*, 548, A25
- Henrard, J., & Murigande, C. 1987, *CeMec*, 40, 345
- Kaasalainen, M., & Torppa, J. 2001, *Icar*, 153, 24
- Kaasalainen, M., Torppa, J., & Muinonen, K. 2001, *Icar*, 153, 37
- Konopliv, A. S., Asmar, S. W., Folkner, W. M., et al. 2011, *Icar*, 211, 401
- Krugly, Y. N. 2004, *SoSyR*, 38, 241
- Margot, J.-L., Pravec, P., Taylor, P., Carry, B., & Jacobson, S. 2015, in *Asteroids IV*, ed. P. Michel, F. E. DeMeo, & W. F. Bottke (Tucson, AZ: Univ. Arizona Press), 355
- Masiero, J. R., Mainzer, A. K., Bauer, J. M., et al. 2013, *ApJ*, 770, 7
- Masiero, J. R., Mainzer, A. K., Grav, T., et al. 2011, *ApJ*, 741, 68
- Milani, A., Cellino, A., Knežević, Z., et al. 2014, *Icar*, 239, 46
- Milani, A., & Gronchi, G. F. 2010, *Theory of Orbital Determination* (Cambridge: Cambridge Univ. Press)
- Mottola, S., De Angelis, G., Di Martino, M., et al. 1995, *Icar*, 117, 62
- Nesvorný, D., & Bottke, W. F. 2004, *Icar*, 170, 324
- Nesvorný, D., Bottke, W. F., Dones, L., & Levison, H. F. 2002, *Natur*, 417, 720
- Nesvorný, D., Brož, M., & Carruba, V. 2015, in *Asteroids IV*, ed. P. Michel, F. E. DeMeo, & W. F. Bottke (Tucson, AZ: Univ. Arizona Press), 297
- Nesvorný, D., Vokrouhlický, D., & Bottke, W. F. 2006, *Sci*, 312, 1490
- Polishook, D. 2014, *Icar*, 241, 79
- Polishook, D., Moskovitz, N., Binzel, R. P., et al. 2014a, *Icar*, 233, 9
- Polishook, D., Moskovitz, N., DeMeo, F. E., & Binzel, R. P. 2014b, *Icar*, 243, 222
- Pravec, P., Harris, A. W., Kušnirák, P., Galád, A., & Hornoch, K. 2012, *Icar*, 221, 365
- Pravec, P., Scheirich, P., Ďurech, J., et al. 2014, *Icar*, 233, 48
- Pravec, P., Scheirich, P., Kušnirák, P., et al. 2006, *Icar*, 181, 63
- Pravec, P., & Vokrouhlický, D. 2009, *Icar*, 204, 580
- Pravec, P., Vokrouhlický, D., Polishook, D., et al. 2010, *Natur*, 466, 1085
- Russell, C. T., Raymond, C. A., Ammannito, E., et al. 2016, *Sci*, 353, 1008
- Russell, C. T., Raymond, C. A., Coradini, A., et al. 2012, *Sci*, 336, 684
- Scheeres, D. J., Britt, D., Carry, B., & Holsapple, K. A. 2015, in *Asteroids IV*, ed. P. Michel, F. E. DeMeo, & W. F. Bottke (Tucson, AZ: Univ. Arizona Press), 745
- Tanga, P., Mignard, F., Dell’Oro, A., et al. 2016, *P&SS*, 123, 87
- Vernazza, P., Binzel, R. P., Rossi, A., Fulchignoni, M., & Birlan, M. 2009, *Natur*, 458, 993
- Vokrouhlický, D. 1998, *A&A*, 335, 1093
- Vokrouhlický, D. 1999, *A&A*, 344, 362
- Vokrouhlický, D., Bottke, W. F., Chesley, S. R., Scheeres, D. J., & Statler, T. S. 2015, in *Asteroids IV*, ed. P. Michel, F. E. DeMeo, & W. F. Bottke (Tucson, AZ: Univ. Arizona Press), 509
- Vokrouhlický, D., Ďurech, J., Polishook, D., et al. 2011, *AJ*, 142, 159
- Vokrouhlický, D., & Farinella, P. 1999, *AJ*, 118, 3049
- Vokrouhlický, D., & Milani, A. 2000, *A&A*, 362, 746
- Vokrouhlický, D., Milani, A., & Chesley, S. R. 2000, *Icar*, 148, 118
- Vokrouhlický, D., & Nesvorný, D. 2008, *AJ*, 136, 280
- Vokrouhlický, D., & Nesvorný, D. 2009, *AJ*, 137, 111
- Vraštil, J. 2015, Master thesis, Charles Univ. Prague
- Vraštil, J., & Vokrouhlický, D. 2015, *A&A*, 579, A14
- Will, C. M. 1993, *Theory and Experiment in Gravitational Physics* (Cambridge: Cambridge Univ. Press)
- Wisdom, J., & Holman, M. 1991, *AJ*, 102, 1528
- Žižka, J., Galád, A., Vokrouhlický, D., et al. 2016, *A&A*, 595, A20
- Žižka, J., & Vokrouhlický, D. 2011, *Icar*, 211, 511